Antarct. Meteorite Res., 12, 213-242, 1999

EVAPORATION OF Fe AND FeS DUST IN THE ACTIVE STAGE OF THE PRIMORDIAL SOLAR NEBULA, AND Fe/S FRACTIONATION

Shogo TACHIBANA[1], Akira TSUCHIYAMA[1] and Sei-ichiro WATANABE[2]

[1] *Department of Earth and Space Science, Graduate School of Science, Osaka University, Machikaneyama, Toyonaka 560-0043*
[2] *Department of Earth and Planetary Science, Graduate School of Science, Nagoya University, Furo-cho, Chikusa-ku, Nagoya 464-0814*

Abstract: The evaporation kinetics of troilite and metallic iron was applied to evaporation of dust particles moving toward the protosun in the turbulent solar nebula. In the calculations, it was assumed that dust particles do not grow by collision, evaporated gas and residual dust are not separated, and dust particles move only radially along the midplane or the surface of the nebula. It was found that evaporation of metallic iron would occur almost in equilibrium both along the midplane and the surface. Troilite could survive to higher temperature than the equilibrium evaporation temperature due to its evaporation kinetics. However, the kinetic effects are not so large, and the incongruent evaporation of troilite is also regarded to occur roughly in equilibrium. The timescales for evaporation of metallic iron and troilite were compared with the timescales for drifts along r- and z-directions and that for coagulation to understand general aspects of the effect of evaporation kinetics. Since the temperature of the surface is lower than that of the midplane, dust particle at the surface can get closer to the sun than those at the midplane. This can cause Fe/S fractionation in a wide range of the nebula if effective solid-gas separation occurred.

1. Introduction

Chondrites are the primitive meteorites which give us a lot of information about the early solar nebula. Their elemental abundance patterns (*e.g.*, DODD, 1981; WASSON and KALLEMEYN, 1988) are different variously from the solar abundance (*e.g.*, ANDERS and GREVESSE, 1989), and have been used for the chemical classification of chondrites (*e.g.*, DODD, 1981; KERRIDGE and MATTHEWS, 1988). It has been also believed that the elemental abundance in the terrestrial planets are different from the solar abundance (*e.g.*, LEWIS, 1995).

The chemical groups of chondrites imply that the elemental fractionation processes must have occurred in the primordial solar nebula. It is widely accepted that the fractionation occurred before chondritic parent bodies were formed (*e.g.*, GROSSMAN and WASSON, 1982, 1983). Note that, however, there are some debates on when the elemental fractionation actually occurred. Some recent studies (*e.g.*, SEARS *et al.*, 1996; HAACK and SCOTT, 1993; SCOTT and HAACK, 1993) suggest that it took place during or after the chondrule formation although it is still open to controversy when and where chondrules were formed.

The elemental fractionation in the primordial solar nebula has been discussed for these three decades by many investigators (*e.g.,* LARIMER and ANDERS, 1967, 1970; LEWIS, 1972; GROSSMAN and LARIMER, 1974). However, most of them have discussed the fractionation based on "the equilibrium condensation model" (*e.g.,* LARIMER and ANDERS, 1967; GROSSMAN, 1972; WOOD and HASHIMOTO, 1993) and the classical physical models for the primordial solar nebula (*e.g.,* CAMERON, 1973). These studies assumed the equilibrium between gas and solid, and could not deal with the time-dependent problems. It is of much importance, however, to consider the kinetics of gas-solid (-liquid) reactions, such as condensation and evaporation, which might have played an important role for the elemental fractionation. Moreover, the temperature of the solar nebula predicted by the classical physical models was high enough to vaporize all dust particles completely in the wide range of the nebula, while recent models for the nebula do not predict such high temperatures (*e.g.,* MORFILL *et al.,* 1985; WATANABE and IDA, 1997). Hence, it is significant to consider the elemental fractionation based on both the reaction kinetics and the recent dynamic models for the formation of the solar nebula.

There are some studies dealing with the condensation kinetics of dust particles in the cooling nebula (*e.g.,* YAMAMOTO and HASEGAWA, 1977; CAMERON and FEGLEY, 1982; LAURETTA *et al.,* 1996; IMAE and KITAMURA, 1995). However, most of those studies considered only the cooling rate of the nebula but dynamic behavior of dust particles in the nebula has not been taken into account. CAMERON and FEGLEY (1982) discussed the nucleation and condensation qualitatively with a solar nebula model of LYNDEN-BELL and PRINGLE (1974). Although they argued the condensation of gas component which moved radially outward and upward from the midplane, respectively, their results had great uncertainties because of the uncertainties in the surface energies of the condensation products. As for evaporation, NAGAHARA and OZAWA (1996) applied their experimental evaporation rates of forsterite to the evaporation behavior of forsterite grains in the solar nebula. They evaluated the lifetime of forsterite dust particles heated at 1700°C in a constant volume, and discussed the possibility of the isotopic fractionation by evaporation as well. However, they did not consider the dynamic movement of dust in the nebula either.

Chondritic parent bodies and planets were formed in the protoplanetary disk (*e.g.,* SHU *et al.,* 1987). In the active stage of the disk, dust particles and gas, which accreted into the disk from a molecular cloud, moved towards the protosun. Hence, the dynamic movement of dust particles should be combined with the reaction kinetics. Moving dust particles to the protosun began to evaporate with increasing the nebular temperature. The partial evaporation of dust particles would cause the compositional difference between gas and solid components. If solid-gas separation occurred effectively, and planets or chondritic parental bodies were formed from such fractionated components, the elemental fractionation should be expected. Accordingly, evaporation is also a responsible process for the elemental fractionation.

Iron and sulfur are the abundant elements forming meteorites and the terrestrial planets in the solar system as well as Mg, Si and O. Fe/S ratios in chondrites except for CI chondrites are larger than that of the solar abundance (Table 1), and indicate Fe/S fractionation in the solar nebula. These fractionations can be explained by the loss of sulfur or the gain of iron. In the case of the terrestrial planets, the Fe/S ratio of the

Table 1. Fe/S ratios [mol] of the solar abundance (ANDERS and GREVESSE, 1989), chondrites (WASSON and KALLEMEYN, 1988) and the bulk Earth (LEWIS, 1995).

Solar	Carbonaceous	Ordinary	Enstatite	Earth
1.75	CI 1.77	H 7.89	EH 2.87	10.58?
	CM 3.65	L 5.61	EL 3.83	
	CO 7.12	LL 4.62		
	CV 6.13			

bulk Earth, for instance, is presumably larger than that of solar abundance although a degree of the loss of sulfur or the gain of iron has not been determined precisely (*e.g.*, LEWIS, 1995). It should be noted that sulfur is one of the moderately volatile elements. The relative abundance pattern of moderately volatile elements decreases more or less monotonically with volatility in chondritic meteorites (PALME *et al.*, 1988). The fractionation of sulfur might be regarded as a part of the elemental fractionation of moderately volatile elements. In the present study, however, we pay attention to Fe/S fractionation as the fractionation of major elements.

The major solid phases of Fe and S in the primitive solar nebula would be metallic iron and troilite (FeS) because they are common phases in meteorites and presumably in the terrestrial planets. With regards to the troilite formation, IMAE and KITAMURA (1995) and LAURETTA *et al.* (1996) discussed the formation reaction in the cooling solar nebula based on the experimental formation rates. Both of them pointed out that the troilite formation was a rapid process and would have occurred nearly at equilibrium in the cooling nebula.

The evaporation kinetics of metallic iron and troilite have been evaluated experimentally by TSUCHIYAMA and FUJIMOTO (1995), TSUCHIYAMA *et al.* (1997) and TACHIBANA and TSUCHIYAMA (1998), respectively. Hence, we can elucidate the evaporation behavior of metallic iron and troilite in the nebula based on their experimental data. Sulfur evaporates selectively from troilite to form metallic iron, and thus evaporation of troilite might have caused Fe/S fractionation in the nebula.

In the present study, in order to elucidate the evaporation behavior of troilite and metallic iron dust particles in the primordial solar nebula and to discuss the Fe/S fractionation caused by evaporation, numerical calculations were carried out by using a recent dynamic model for the formation of the primordial solar nebula (WATANABE and IDA, 1997) combined with evaporation kinetics of troilite (TACHIBANA and TSUCHIYAMA, 1998) and metallic iron (TSUCHIYAMA and FUJIMOTO, 1995).

2. Nebula Model

WATANABE and IDA's model (1997) used in this calculation is the one for a turbulent protoplanetary disk. The active turbulent nebula is assumed to be in a steady state where the infall flux of matter from the molecular cloud balances with the accretion flux through the nebula to the sun. In this model, conditions of the nebula, such as the surface density, Σ_g, temperature of the midplane, T_m, and that of the surface, T_s, are

Table 2. Four different nebular conditions used for the present calculations. $\dot{M}/M_\odot$, α_ν and $L_\bullet/L_\odot$ are parameters of WATANABE and IDA's model. Σ_g, T_m and T_s in their model were approximated to power functions of r/r_0, where r is the distance from the protosun, and r_0 corresponds to 1 AU.

[Model 1] ($\dot{M}=1.0\times10^{-7}M_\odot$ yr^{-1}, $\alpha_\nu=0.001$, $L_\bullet=10L_\odot$)		
Σ_g(g cm^{-3})	$3500\ (r/r_0)^{-0.88}$	
p_{total} (bar)	$3.85\times10^{-5}(r/r_0)^{-2.68}$	$(r/r_0>6)$
	$5.46\times10^{-5}(r/r_0)^{-2.88}$	$(0.8<r/r_0\leq6)$
	$5.93\times10^{-5}(r/r_0)^{-2.51}$	$(r/r_0\leq0.8)$
T_m (K)	$585\ (r/r_0)^{-0.61}$	$(r/r_0>6)$
	$1176\ (r/r_0)^{-1}$	$(0.8<r/r_0\leq6)$
	$1387\ (r/r_0)^{-0.26}$	$(r/r_0\leq0.8)$
T_s (K)	$275\ (r/r_0)^{-0.45}$	$(r/r_0>6)$
	$296\ (r/r_0)^{-0.49}$	$(0.8<r/r_0\leq6)$
	$286\ (r/r_0)^{-0.64}$	$(r/r_0\leq0.8)$
v_r (cm s^{-1})	$19.1\ (r/r_0)^{-0.12}$	

[Model 2] ($\dot{M}=1.0\times10^{-7}M_\odot$ yr^{-1}, $\alpha_\nu=0.01$, $L_\bullet=10L_\odot$)		
Σ_g(g cm^{-3})	$440\ (r/r_0)^{-0.92}$	
p_{total} (bar)	$4.00\times10^{-6}(r/r_0)^{-2.68}$	$(r/r_0>3)$
	$5.21\times10^{-6}(r/r_0)^{-2.91}$	$(0.5<r/r_0\leq3)$
	$6.69\times10^{-6}(r/r_0)^{-2.56}$	$(r/r_0\leq0.5)$
T_m (K)	$400\ (r/r_0)^{-0.52}$	$(r/r_0>3)$
	$678\ (r/r_0)^{-1}$	$(0.5<r/r_0\leq3)$
	$1117\ (r/r_0)^{-0.28}$	$(r/r_0\leq0.5)$
T_s (K)	$264\ (r/r_0)^{-0.44}$	$(r/r_0>3)$
	$292\ (r/r_0)^{-0.53}$	$(0.5<r/r_0\leq3)$
	$267\ (r/r_0)^{-0.66}$	$(r/r_0\leq0.5)$
v_r (cm s^{-1})	$152.1\ (r/r_0)^{-0.08}$	

[Model 3] ($\dot{M}=1.0\times10^{-7}M_\odot$ yr^{-1}, $\alpha_\nu=0.1$, L$_\bullet=10L_\odot$)		
Σ_g(g cm^{-3})	$52\ (r/r_0)^{-0.96}$	
p_{total} (bar)	$4.46\times10^{-7}(r/r_0)^{-2.71}$	$(r/r_0>1.4)$
	$4.85\times10^{-7}(r/r_0)^{-2.96}$	$(0.3<r/r_0\leq1.4)$
	$7.40\times10^{-7}(r/r_0)^{-2.60}$	$(r/r_0\leq0.3)$
T_m (K)	$355\ (r/r_0)^{-0.50}$	$(r/r_0>1.4)$
	$420\ (r/r_0)^{-1}$	$(0.3<r/r_0\leq1.4)$
	$1049\ (r/r_0)^{-0.24}$	$(r/r_0\leq0.3)$
T_s (K)	$267\ (r/r_0)^{-0.44}$	$(r/r_0>1.4)$
	$279\ (r/r_0)^{-0.57}$	$(0.3<r/r_0\leq1.4)$
	$239\ (r/r_0)^{-0.70}$	$(r/r_0\leq0.3)$
v_r (cm s^{-1})	$1287\ (r/r_0)^{-0.04}$	

[Model 4] ($\dot{M}=1.0\times10^{-6}M_\odot$ yr^{-1}, $\alpha_\nu=0.01$, $L_\bullet=10L_\odot$)		
Σ_g(g cm^{-3})	$3000\ (r/r_0)^{-0.84}$	
p_{total} (bar)	$2.9\times10^{-6}(r/r_0)^{-2.44}$	$(r/r_0>9)$
	$2.28\times10^{-6}(r/r_0)^{-2.35}$	$(1.3<r/r_0\leq9)$
	$2.64\times10^{-6}(r/r_0)^{-2.86}$	$(r/r_0\leq1.3)$
T_m (K)	$1005\ (r/r_0)^{-0.50}$	$(r/r_0>9)$
	$1944\ (r/r_0)^{-1}$	$(1.3<r/r_0\leq9)$
	$1573\ (r/r_0)^{-0.24}$	$(r/r_0\leq1.3)$
T_s (K)	$318\ (r/r_0)^{-0.45}$	$(r/r_0>9)$
	$362\ (r/r_0)^{-0.51}$	$(1.3<r/r_0\leq9)$
	$377\ (r/r_0)^{-0.66}$	$(r/r_0\leq1.3)$
v_r (cm s^{-1})	$223.1\ (r/r_0)^{-0.16}$	

$\dot{M}$: steady accretion rate of mass towards the protosun,
α_ν: α parameter which defines the turbulence viscosity of the nebula,
$L_\bullet$: luminosity of the protosun, Σ_g: the surface density of gas,
p_{total}: total pressure, T_m: temperature of the midplane,
T_s: temperature of the surface, v_r: drift velocity of dust and gas.

obtained by numerical calculations as a function of the steady accretion rate of mass, $\dot{M}$, the luminosity of the protosun, $L_\bullet$, and α_ν parameter for the turbulent viscosity. The Rosseland mean opacity in RUDEN and POLLACK (1991) was also used to obtain T_m and T_s. In the present calculations, Σ_g, T_m and T_s, were approximated to power functions of the distance from the protosun, r (Table 2);

$$f_i = A_i (r/r_0)^{x_i} \qquad (i = \Sigma_g, T_m \text{ or } T_s), \tag{1}$$

where r_0 is the distance from the sun to the Earth. Other nebular parameters including total pressure can be derived from these primary relations of $\Sigma_g(r)$, $T_m(r)$ and $T_s(r)$.

Drift velocity, v_r, is calculated from $\dot{M}$ and Σ_g;

$$v_r = \frac{\dot{M}}{2\pi r \cdot \Sigma_g}. \tag{2}$$

The scale height, h, in the adiabatic nebula (from the midplane to the surface) is expressed by

$$h = \sqrt{\frac{2\gamma}{\gamma - 1} \frac{kT_m}{\mu \Omega_k^2}}, \tag{3}$$

where γ is a ratio between the heat capacity at constant pressure and that at constant volume, k, the Boltzmann constant, and μ, the mean molecular weight of nebular gas ($2.34 m_H$; m_H is the mass of hydrogen atom). The surface density of dust, Σ_d, is expressed by Σ_g;

$$\Sigma_d = 4.3 \times 10^{-3} \Sigma_g, \tag{4}$$

where the constant (4.3×10^{-3}) is a ratio between dust and gas in the region in which icy dust particles completely evaporate. The densities of gas and dust particles in the midplane, $\rho_{mid,g}$ and $\rho_{mid,d}$, respectively, are given by

$$\rho_{mid,g} = \frac{16\Sigma_g}{5\pi h}, \text{ and } \rho_{mid,d} = \frac{16\Sigma_d}{5\pi h}, \tag{5}$$

and those in the surface, $\rho_{sur,g}$ and $\rho_{sur,d}$, are given by

$$\rho_{sur,g} = \frac{\Sigma_g}{\sqrt{\pi}\, he}, \text{ and } \rho_{sur,d} = \frac{\Sigma_d}{\sqrt{\pi}\, he}, \tag{6}$$

where e is the base of the natural logarithms.

Four different nebular conditions (Models 1–4) were used for the present calculations (Table 2, Fig. 1). L_* is fixed in all the models ($10 L_\odot$), and $\dot{M}$ is same in Models 1–3 ($1.0 \times 10^{-7} M_\odot$ yr^{-1}), while $\dot{M}$ in Model 4 is larger than the others (1.0×10^{-6} $M_\odot$ yr^{-1}). The values of α_ν, which is a parameter to define the turbulent viscosity, are 0.001 for Model 1, 0.01 for Models 2 and 4 and 0.1 for Model 3, respectively. Larger α_ν values correspond to the stronger turbulent viscosity, and thus Σ_g and T_m decrease in this order as long as $\dot{M}$ is same (Models 1, 2, and 3 in Figs. 1a and 1b). The temperatures are higher in Model 4 because $\dot{M}$ is larger than others (Fig. 1b). The values of v_r depend on Σ_g and $\dot{M}$ (eq. 2), and are the largest and smallest in Model 3 and 1,

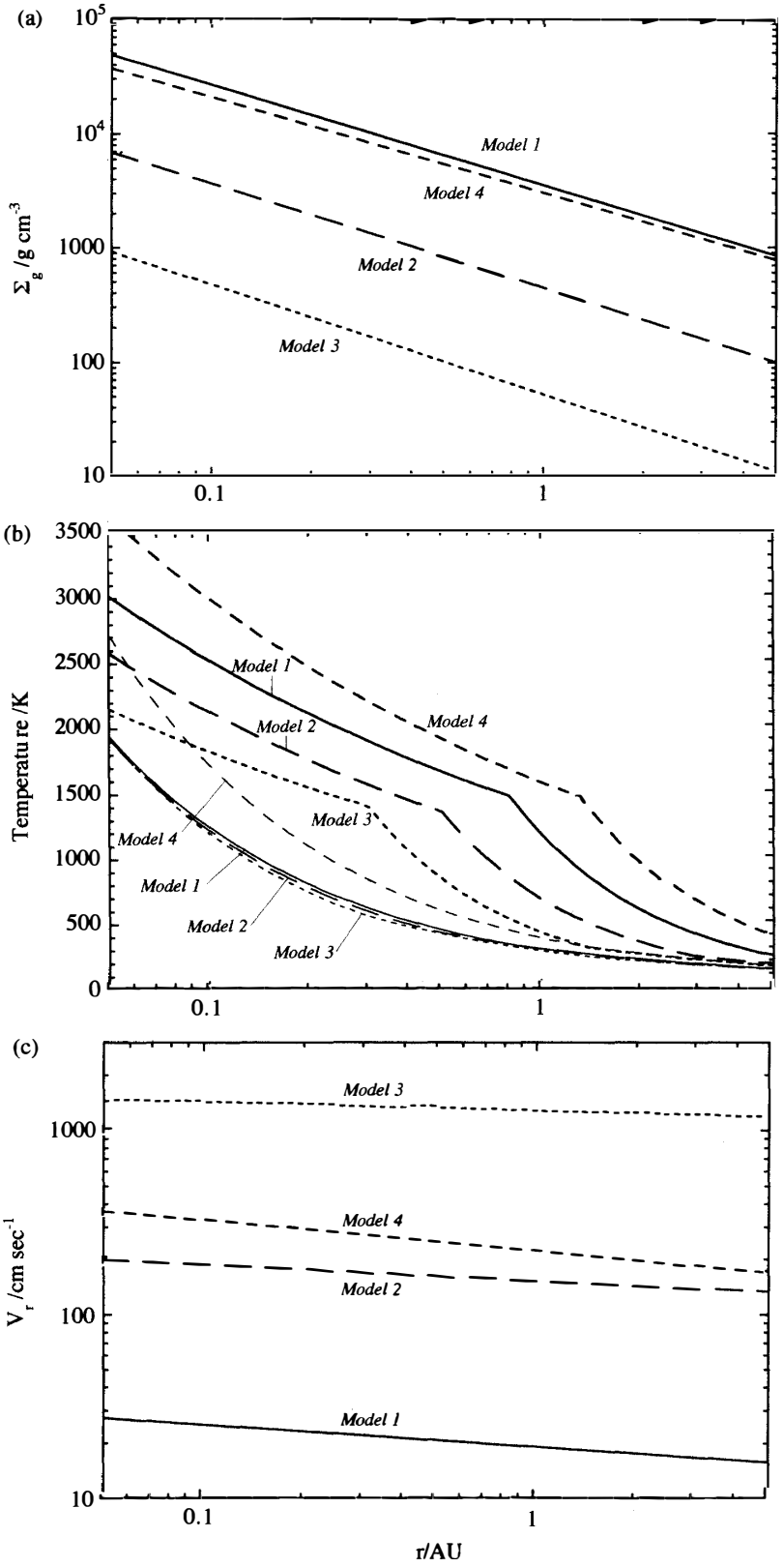

Fig. 1. Nebular parameters plotted against the distance from the protosun, r, in Models 1–4 (Table 1). (a) Surface density of gas, Σ_g. (b) Temperature along the midplane, T_m, and surface, T_s. Thick lines represent T_m, and thin lines, T_s. (c) Drift velocity of dust and gas, v_r.

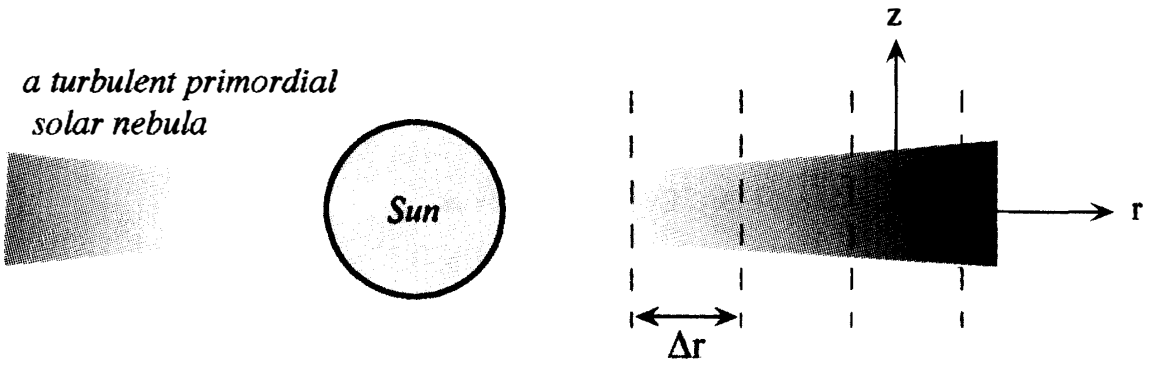

Fig. 2. A schematic drawing of a turbulent primordial solar nebula. The nebula was divided into cells ($\Delta r = 0.01$–10^{-5} AU) both along the midplane and the surface in r-direction for the numerical calculations.

respectively (Fig. 1c).

The following assumptions were made for the present calculations to simplify the problem; (1) the changes in nebular conditions by evaporation of ice, silicate and metal dust, which are taken into account a priori in the present model, are not affected by the evaporation of Fe and FeS dust in this calculation, (2) dust particles (initially 100 or 1 μm in size) do not grow or break by collision, and the fine dust particles and evaporated gas move together with the same drift velocity, v_r, without separation, (3) gas diffusion to the outer region, which is induced by the pressure gradient, is not considered, (4) dust particles do not move along z-direction (from the midplane to the nebular surface) but move only along r-direction (from the outer part of the nebula to the sun) (Fig. 2), (5) Fe, S, H and He in the nebula have the ratios of the solar elemental abundance (ANDERS and GREVESSE, 1989), and (6) pure Fe metal and troilite (FeS) are considered as metal and sulfide phases, respectively. As for the assumption (1), the Rosseland mean opacity used in the present model (RUDEN and POLLACK, 1991) contains the effect of the evaporation of major opacity-bearing materials, such as ice, silicates, and metallic iron, a priori with taking equilibrium evaporation temperatures into account. Evaporation of metallic iron, which is a major source of the opacity, would change the temperature distribution in the nebula, and this would be inconsistent with the assumption (1). The assumption (1) means that the evaporation behavior of Fe and FeS dust particles is investigated in the present study by putting test particles into the disk with the temperature distribution specified by the disk model. The validity of the assumption (1) is discussed later again. Although we do not calculate numerically the kinetic effect of evaporation along z-direction as in the assumption (4), we will make a rough approximation of the material distribution in the nebula by taking the z-direction mixing into account based on the present result. The assumption (6) is, strictly speaking, incorrect for metal. Because metal in meteorites contains Ni in general, the evaporation of Fe-Ni metal should be considered in fact. However, we cannot do that at present because of the lack of the experimental data for the evaporation of Fe-Ni metal. As for sulfides, Fe-Ni sulfide might be a primary sulfide phase in the solar nebula as suggested by LAURETTA *et al.* (1997). If this is the case, we should take account of the

evaporation of Fe-Ni sulfide instead of troilite. However, because the evaporation of sulfur from Fe-Ni sulfide leads to form Fe-Ni metal and troilite (TACHIBANA and TSUCHIYAMA, unpublished data; LAURETTA, 1997), the assumption (6) seems to be plausible for sulfides.

3. Evaporation Rates

3.1. *Fe*

The evaporation reaction of metallic iron can be expressed as follows (TSUCHIYAMA and FUJIMOTO, 1995);

$$Fe(s) = Fe(g), \tag{7}$$

where s and g denote solid and gas, respectively. In this reaction, it is assumed that $Fe(g)$, molecular species in equilibrium with $Fe(s)$, is formed by the evaporation. The evaporation rate of metallic iron is expressed by the Hertz-Knudsen equation (*e.g.*, HIRTH and POUND, 1963; PAULE and MARGRAVE, 1967);

$$J(Fe) = \frac{\alpha [p^e(Fe) - p(Fe)]}{\sqrt{2\pi m_{Fe} kT}}, \tag{8}$$

where $p^e(Fe)$ is an equilibrium pressure of $Fe(g)$, $p(Fe)$, a partial pressure of $Fe(g)$ in the nebula, m_{Fe}, the atomic weight of iron, k, the Boltzmann constant, T, temperature and α (≤ 1), the evaporation coefficient, which shows kinetic constraints for evaporation. The value of α is approximately unity in case of the evaporation of metallic iron (TSUCHIYAMA and FUJIMOTO, 1995).

According to the equilibrium condensation theory (*e.g.*, GROSSMAN, 1972), metallic iron should be oxidized to form magnesium-iron silicates, such as olivine and pyroxene, at low temperatures ($\leq 500-700$K). Such an oxidation effect was not considered in the present calculation.

3.2. *FeS*

It is known that sulfur evaporates selectively from troilite (incongruent evaporation) since sulfur is more volatile than iron. Such incongruent evaporation rates of troilite under the primordial solar nebular conditions were elucidated by TACHIBANA and TSUCHIYAMA (1998) based on their experiments carried out at 800–970°C and 10^{-6}-1atm of hydrogen pressure, $p(H_2)$. A porous iron layer is formed as the evaporation residue, and the evaporation reaction proceeds lineally with time (a linear rate law). They concluded that the evaporation as $H_2S(g)$;

$$FeS(s) + H_2(g) = Fe(s) + H_2S(g), \tag{9}$$

takes place in a high total pressure (or $p(H_2)$) and low temperature region, while the evaporation as $S_2(g)$;

$$FeS(s) = Fe(s) + 1/2 S_2(g), \tag{10}$$

and probably as $HS(g)$;

$$FeS(s) + 1/2 H_2(g) = Fe(s) + HS(g), \tag{11}$$

occur in a low total pressure and high temperature region. Because the evaporation reaction of eq. (9) is suppressed by a sluggish reaction between hydrogen and the troilite surface, the evaporation reaction of eq. (10) becomes important even in regions where the most abundant equilibrium S-bearing gas species in the Fe-S-H system is $H_2S(g)$. We adopted their model-(A), where only the flux of H_2S and S_2 are considered, and the evaporation coefficients, α, of the evaporation reactions of eqs. (9)and (10)are constant under all p-T conditions, in the present calculations for simplicity. Thus, the evaporation flux of sulfur from troilite is expressed as follows;

$$J(S) = J(S)_{H_2S} + J(S)_{S_2} = \frac{\alpha_{H_2S} q [p^e(H_2S) - p(H_2S)]}{\sqrt{2\pi m_{H_2S} kT}} + \frac{2\alpha_{S_2} q [p^e(S_2) - p(S_2)]}{\sqrt{2\pi m_{S_2} kT}}, \tag{12}$$

where $p^e(H_2S)$ and $p^e(S_2)$ are equilibrium pressures of $H_2S(g)$ and $S_2(g)$, respectively, $p(H_2S)$ and $p(S_2)$, partial pressures of $H_2S(g)$ and $S_2(g)$ in the solar nebula, respectively, m_{H_2S} and m_{S_2}, the molecular weights of H_2S and S_2, respectively, and q, the proportion of surface area of troilite (a part of the surface of troilite is covered with residual metallic iron). The values of α_{H_2S} and α_{S_2} of 9.5×10^{-4} and 0.23, respectively, determined from their data at 800–970°C are adopted, and extrapolated to lower temperatures. The value of q was assumed to be constant (0.609) and equal to the porosity expected for evaporation of only sulfur from troilite without changing the original size of troilite under all calculated conditions. It should be noted that TACHIBANA and TSUCHIYAMA (1998) used mm-sized single crystals of troilite in their experiments, while the present calculations consider 100 and 1 μm sized troilite particles. They also carried out an evaporation experiment on about 10–100 μm sized particles of troilite, and found that residual iron did not cover the whole surface of troilite but a part of it. This indicates that troilite dust particles also evaporate following a linear rate law similar as in the experiments using mm-sized crystals.

4. Calculations

4.1. Fe

Calculations in the case of metallic iron were carried out for two different sized dust particles (100 and 1 μm) which move along the midplane and the surface, respectively, based on the following algorithm.

(I) The total density of Fe including $Fe(s)$ and $Fe(g)$, ρ_t^{Fe}, is assumed to be equal to $0.32\rho_{\mathrm{mid,d}}$ and $0.32\rho_{\mathrm{surf,d}}$ Hereafter, the subscripts, mid. and surf., are omitted for simplicity. The constant of 0.32 is the proportion of Fe in the refractory dust (Fe and

silicates) based on the solar abundance (ANDERS and GREVESSE, 1989). The proportion of Fe dust to the total Fe, f_{Fe}, is expressed by

$$f_{Fe}=\rho_d^{Fe}/\rho_t^{Fe}=1-\frac{\rho_g^{Fe}}{\rho_t^{Fe}}, \tag{13}$$

where ρ_d^{Fe} and ρ_g^{Fe} are densities of iron dust and gas, respectively. The partial pressure of Fe, $p(Fe)$, can be calculated from f_{Fe} and ρ_t^{Fe} based on eq. (13) with the ideal gas assumption.

(II) The turbulent nebula was divided into cells, Δr (0.01–10^{-5} AU), in r-direction (Fig. 2).

(III) Dust particles and gas stay in an i-th cell, cell (i), for duration, $\Delta t\,(i)$ ($=\Delta r/v_r\,(i)$). In the cell, metallic iron particles evaporate with the flux, $J(Fe)$ (eq. 8), for $\Delta t\,(i)$. The new f_{Fe} and $p(Fe)$ in the cell are calculated by using f_{Fe} and $p(Fe)$ in the former cell $(i-1)$ with the procedures described below to satisfy the steady state conditions.

(IV) The change of ρ_d^{Fe} caused by the evaporation in cell (i), $\Delta\rho_d^{Fe}\,(i)$, is given by

$$\Delta\rho_d^{Fe}\,(i)=J\,(Fe)\cdot 4\pi D\,(i-1)^2\cdot N_{Fe}\,(i)\cdot m_{Fe}\cdot\Delta t\,(i), \tag{14}$$

where $D\,(i-1)$ is the radius of dust in cell $(i-1)$, and $N_{Fe}\,(i)$ is the number density of metallic iron dust particles. $N_{Fe}\,(i)$ is expressed by

$$N_{Fe}(i)=N_{Fe}(i)=\frac{\rho_d^{Fe}(i)}{\frac{4}{3}\pi D(i-1)^3\cdot\tilde{\rho}_{Fe}}, \tag{15}$$

where $\tilde{\rho}_{Fe}$ is a material density of metallic iron (7.88 g/cm^3; CARMICHAEL, 1989), and $f_{Fe}\,(i)$ before evaporation of iron in cell (i) is given by

$$f_{Fe}\,(i)=\frac{D\,(i-1)^3}{D_0^3}, \tag{16}$$

where D_0 is an initial radius of metallic iron dust particles (100 or 1 μm). Because a change of f_{Fe} in cell (i) due to evaporation of metallic iron, $\Delta f_{Fe}\,(i)$, is related to $\Delta\rho_d^{Fe}(i)$ by

$$\Delta\rho_d^{Fe}\,(i)=\rho_d^{Fe}\ \Delta f_{Fe}(i), \tag{17}$$

$\Delta f_{Fe}\,(i)$ can be expressed from eqs. (14)–(16) as follows;

$$\Delta f_{Fe}\,(i)=3J(Fe)\cdot f_{Fe}(i)^{\frac{2}{3}}\cdot\frac{m_{Fe}}{\tilde{\rho}_{Fe}D_0}\cdot\Delta t(i). \tag{18}$$

After evaporation in cell (i), $f_{Fe}(i)$ is changed to $f'_{Fe}(i)=f_{Fe}(i)+\Delta f_{Fe}(i)$. $f'_{Fe}(i)$ is compared with the equilibrium proportion of Fe dust, $f^{eq}_{Fe}(i)$;

$$f^{eq}_{Fe}=1-\frac{m_{Fe}p^{e}_{Fe}(i)}{\rho^{Fe}_{t}(i)\,k\,T_{m(s)}(i)}, \tag{19}$$

where $p^{e}_{Fe}(i)$ is the equilibrium pressure of $Fe(g)$ in cell (i) calculated by using thermodynamic data (CHASE *et al.*, 1985).

(V) If $f'_{Fe}(i)$ is larger than $f^{eq}_{Fe}(i)$, the equilibrium is not reached by the evaporation in cell (i), and thus the value of $f'_{Fe}(i)$ is used in the next inner cell $(i+1)$ as $f_{Fe}(i+1)$. On the other hand, if $f'_{Fe}(i)$ is smaller than $f^{eq}_{Fe}(i)$, the equilibrium is reached in cell (i), and thus the value of $f^{eq}_{Fe}(i)$ is used in the next inner cell $(i+1)$ as $f_{Fe}(i+1)$.

4.2. *FeS*

Calculations for FeS are essentially similar to those for Fe, but slightly complex because the two kinds of evaporation flux of H_2S and S_2 are taken into consideration (eq. 12). The total density of FeS, ρ^{FeS}_{t}, is assumed to be equal to $0.26\rho_d$ based on the solar abundance (ANDERS and GREVESSE, 1989). The constant of 0.26 is the proportion of FeS in the dust (Fe, FeS and silicates). A change of f_{FeS} in cell (i) due to incongruent evaporation of troilite, $\Delta f_{FeS}(i)$, is expressed by

$$\Delta f_{FeS}(i)=\Delta f^{H_2S}_{FeS}(i)+\Delta f^{S_2}_{FeS}(i)=3\,[J(H_2S)+2J(S_2)]\cdot f_{FeS}(i)^{\frac{2}{3}}\cdot\frac{m_{FeS}}{\tilde{\rho}_{FeS}D_0}\cdot\Delta r(i), \tag{20}$$

where $\Delta f^{H_2S}_{FeS}(i)$ and $\Delta f^{S_2}_{FeS}(i)$ are changes in f_{FeS} due to evaporation as $H_2S(g)$ and $S_2(g)$, respectively, from troilite, $\tilde{\rho}_{FeS}$ is a material density of troilite (4.830 g/cm^3; CARMICHAEL, 1989), and m_{FeS}, the molecular weight of FeS. $\Delta f^{H_2S}_{FeS}(i)$ and $\Delta f^{S_2}_{FeS}(i)$ are compared with the changes in f_{FeS} for the troilite-iron-gas equilibrium, $\Delta f^{H_2S,eq}_{FeS}(i)$ and $\Delta f^{S_2,eq}_{FeS}(i)$, respectively;

$$\Delta f^{H_2S,eq}_{FeS}(i)=f_{FeS}(i)-\left(1-\frac{K}{2\cdot([S]/[H])_{\text{solar}}}\right), \tag{21}$$

$$\Delta f^{S_2,eq}_{FeS}(i)=f_{FeS}(i)-\left(1-\frac{m_{S_2}p^{eq}_{S_2}(i)}{2\rho^{FeS}_{t}(i)\,kT_{m(s)}(i)}\right), \tag{22}$$

where $([S]/[H])_{\text{solar}}$ is the atomic abundance ratio of H and S in the solar system (ANDERS and GREVESSE, 1989), and K is the equilibrium constant of the reaction expressed by eq. (9). If $\Delta f^{H_2S}_{FeS}(i)$ (or $\Delta f^{S_2}_{FeS}(i)$) is larger than $\Delta f^{H_2S,eq}_{FeS}(i)$ (or $\Delta f^{S_2,eq}_{FeS}(i)$), $\Delta f^{H_2S,eq}_{FeS}(i)$ (or $\Delta f^{S_2,eq}_{FeS}(i)$) is used as the change in f_{FeS}.

If the total evaporation of H_2S and S_2 does not reach an equilibrium state, partial pressures of H_2S and S_2 are accommodated to obtain the following H_2S-S_2 equilibrium in cell (i);

$$H_2(g) + 1/2 S_2(g) = H_2S(g). \quad (23)$$

$p(H_2S)$ and $p(S_2)$ obtained from $\Delta f_{FeS}^{H_2S}(i)$ and $\Delta f_{FeS}^{S_2}(i)$, respectively, are changed to satisfy the following equation;

$$K' = \frac{p(H_2)\sqrt{p(S_2)}}{p(H_2S)}, \quad (24)$$

where K' is the equilibrium constant of eq. (23). Since $p(H_2)$ is much larger than $p(H_2S)$ and $p(S_2)$ in eq. (24) under the present calculated conditions, the value of $p(H_2)$ is treated as a constant which is calculated from ρ_g by assuming that the nebula gas is ideal and total pressure is the sum of $p(H_2)$ and $p(He)$ with the H/He ratio of the solar abundance (ANDERS and GREVESSE, 1989). Those accommodated $p(H_2S)$ and $p(S_2)$ are used as the partial pressures in the next inner cell $(i+1)$.

4.3. *Equilibrium calculations*

In addition to the calculations for the evaporation behavior, solid-gas equilibria under the present nebular conditions were calculated for metallic iron and troilite dust. In these calculations, the solar abundance of H, He, Fe and S based on ANDERS and GREVESSE (1989) was assumed for consistency with the evaporation calculations. $Fe(s)$, $FeS(s)$, $H_2(g)$, $He(g)$, $Fe(g)$, $H_2S(g)$ and $S_2(g)$ were taken into consideration with thermodynamic data of CHASE *et al.* (1985). Therefore, the results should be the same as those by the above evaporation calculations in which the initial size of the dust is infinitesimal (or the evaporation rate is infinite).

4.4. *Dust enriched conditions*

The turbulence might have swept dust particles and concentrated them in the eddy of the turbulent gas (CUZZI *et al.*, 1996). CUZZI *et al.* (1996) proposed that the chondrule formation occurred in those regions and chondrules were made from those concentrated dust particles. To evaluate the kinetic effects on the evaporation of concentrated dust particles, we used a dust enrichment factor, η, and simulated the evaporation behavior of dust particles which have the density, $\eta\rho_d$, by using Model 2. Other parameters for the calculation of evaporation kinetics were the same as those described above. In the equilibrium calculations, $\eta([Fe]/[H])_{solar}$ and $\eta([S]/[H])_{solar}$ were substituted for the solar elemental ratios, $([Fe]/H)_{solar}$ and $([S]/[H])_{solar}$, respectively.

5. Results

The results of calculations for the solar elemental ratios ($\eta = 1$) with the equilibrium calculations are shown in Figs. 3 and 4. In these figures, the dust/(gas+dust) ratios (*e.g.*, f_{Fe} of eq. (13) for Fe) are plotted against the distance from the sun, r, for the four nebula models (Models 1–4 in Table 1). For example, in the case of metallic

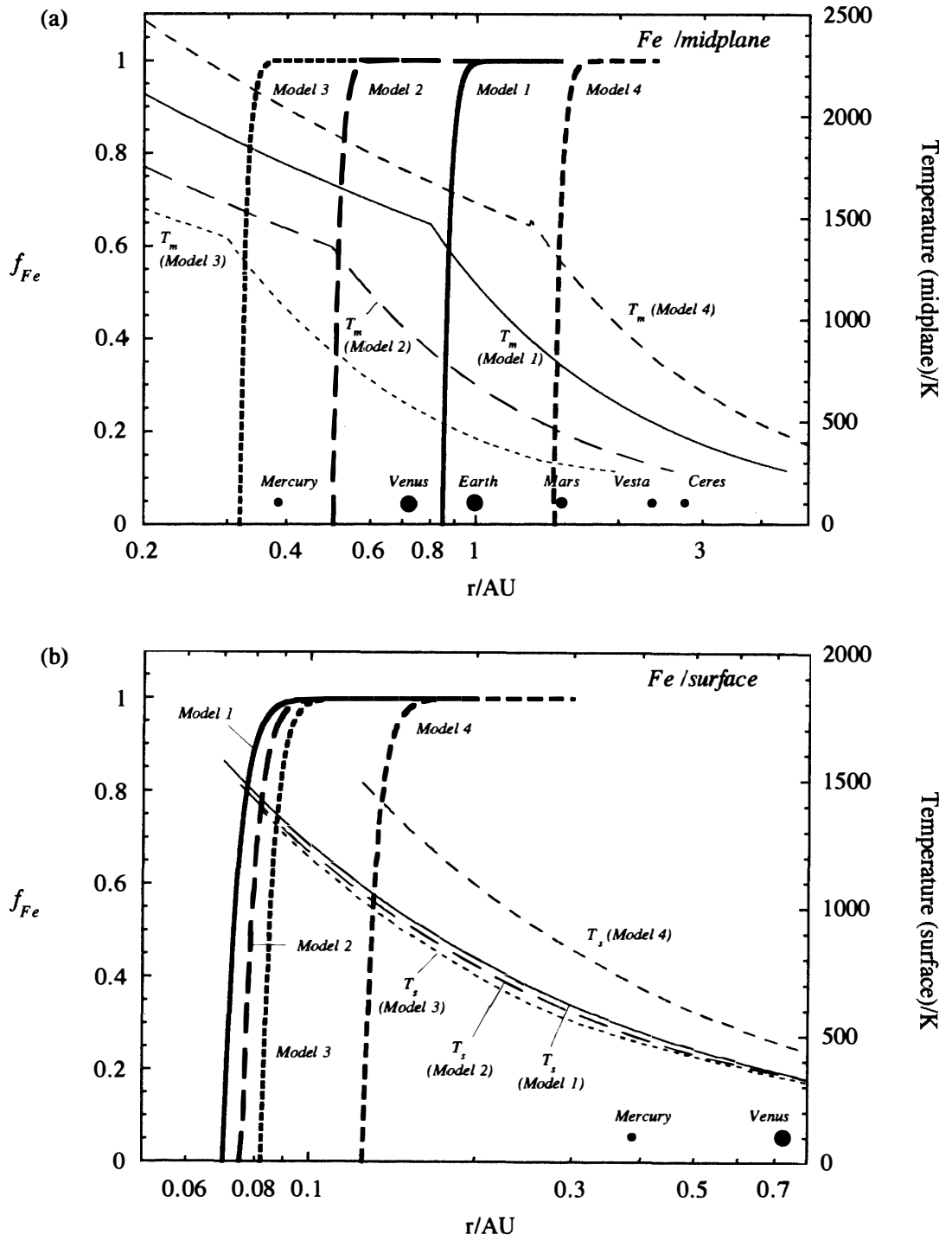

Fig. 3. The calculated dust/(dust+gas) ratios of Fe ($D_0=1$ and 100 μm) by evaporation, f_{Fe}, plotted against the distance from the sun, r, based on WATANABE *and* IDA*'s models (Model 1–4). (a) Dust moving along the midplane of the nebula. (b) Dust moving along the surface of the nebula. Evaporation curves with $D_0=1$ and 100 μm and the curve in the case of equilibrium cannot be distinguished in each model Thus, these evaporation curves are drawn by single curves. Temperatures in the four models are superimposed. The orbits of planets and asteroids are also shown.*

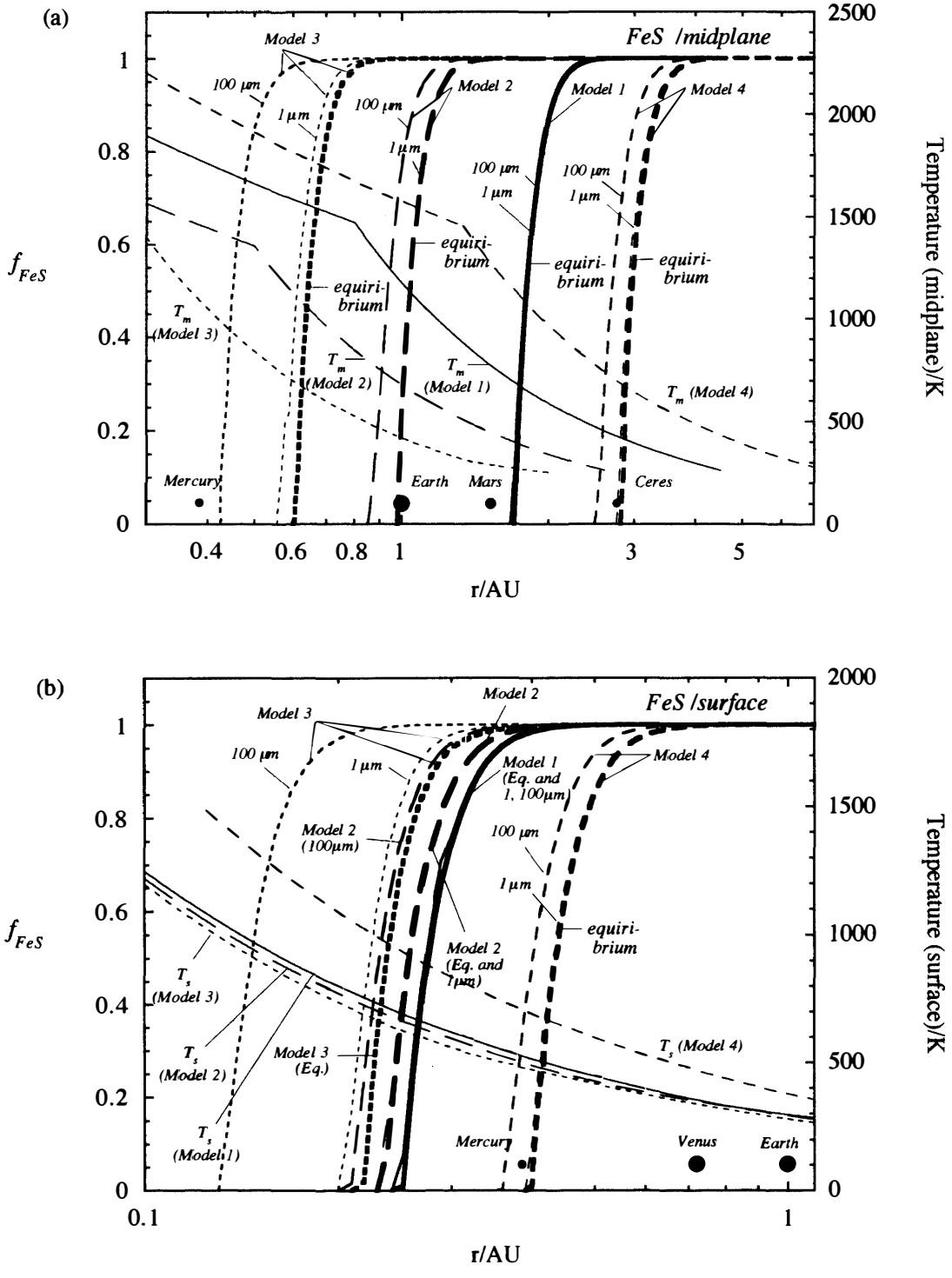

Fig. 4. The calculated dust/(dust+gas) ratios of FeS (D_0=1 and 100 μm) by incongruent evaporation, f_{FeS}, plotted against the distance from the sun, r, based on WATANABE *and* IDA*'s models (Model 1-4). (a) Dust moving along the midplane of the nebula. (b) Dust moving along the surface of the nebula. Evaporation curves with initial dust radius, D_0, of 1 and 100 μm and the curve in the case of equilibrium (thick lines) are shown. Temperatures in the four models are also superimposed. The orbits of planets and asteroids are also shown.*

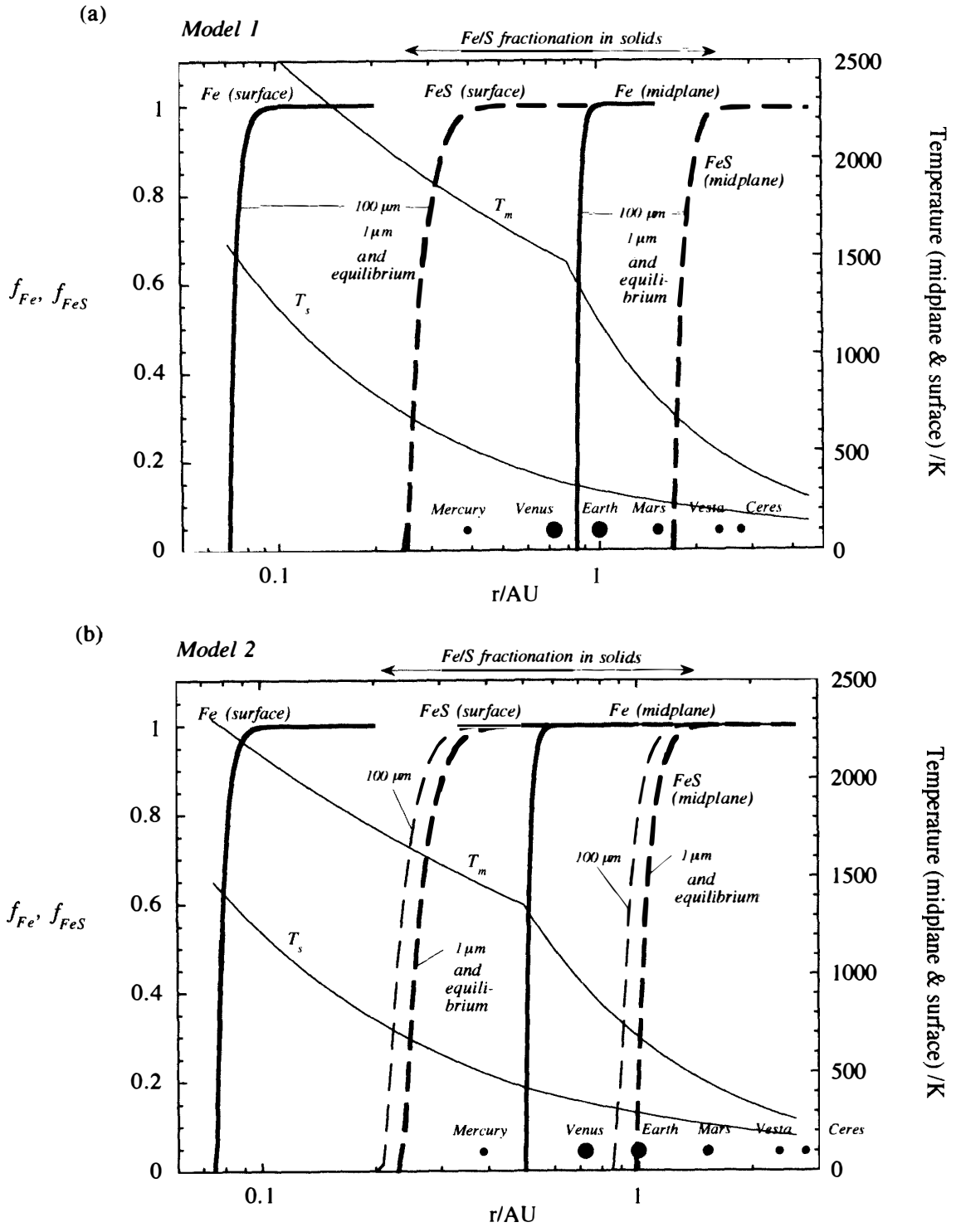

Fig. 5. The calculated dust/(dust+gas) ratios of Fe and FeS ($D_0=1$ and 100 μm and equilibrium case) along the midplane and surface of the nebula plotted against the distance from the sun, r. (a) Model 1. (b) Model 2. (c) Model 3. (d) Model 4. The expected range for Fe/S fractionation in solid components is also shown. T_m; temperature of the midplane, and T_s; temperature of the surface.

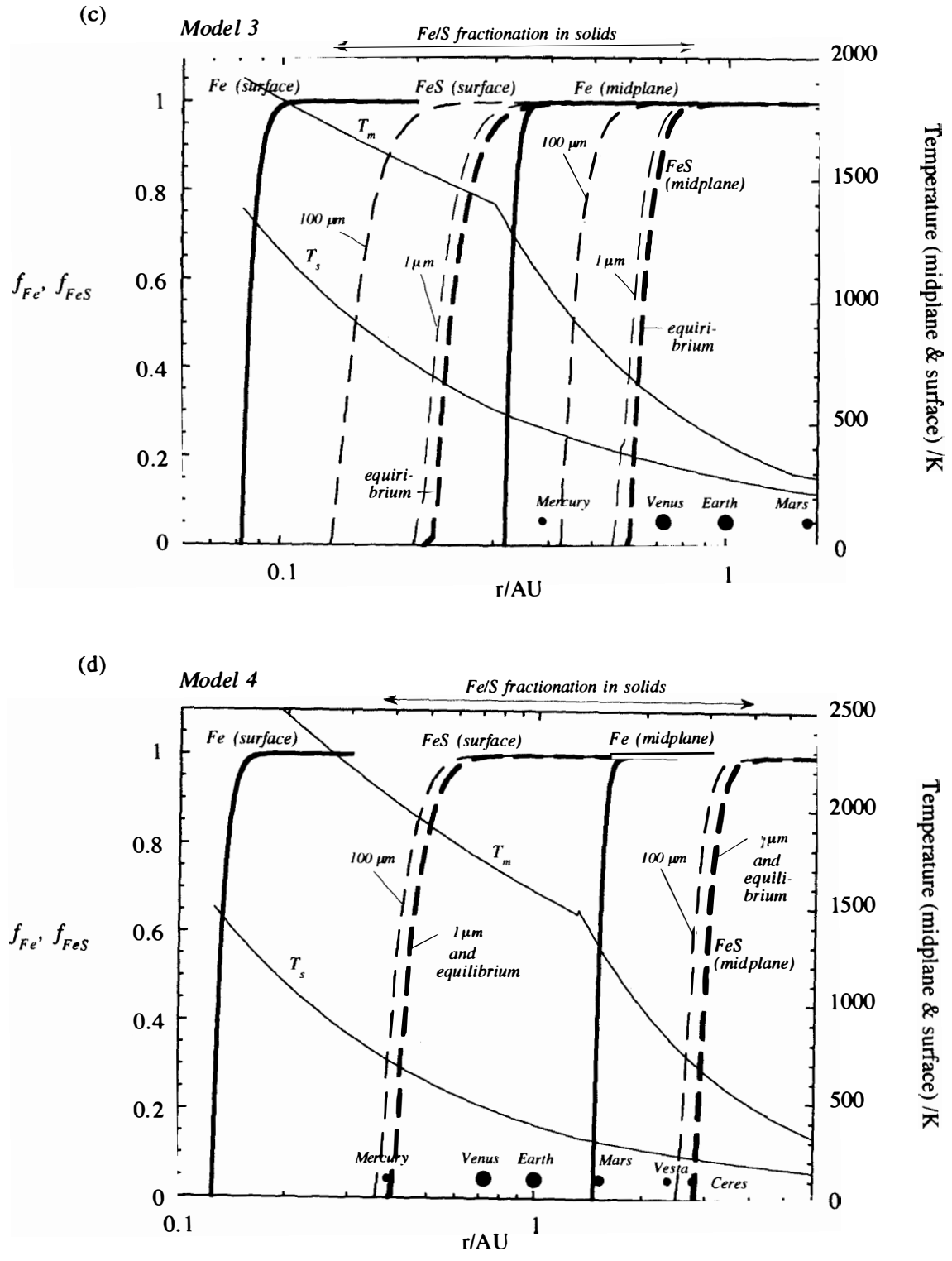

Fig. 5 (continued).

iron along the midplane of Model 1 (Fig. 3a), metallic iron dust falling towards the sun starts to evaporate at $r \approx 1.0$ AU and evaporates completely at $r \approx 0.83$ AU. The f_{Fe}-r curves with $D_0 = 1$ and 100 μm and the equilibrium curve cannot be distinguished from each other irrespective of the models. The evaporation region along the midplane (*e.g.*, $r = 1.0$–0.83 AU for Model 1) changes in accordance with the temperature distribution along the midplane, $T_m(r)$ (Fig. 3a). Metallic iron evaporates near the Mars's orbit in the model with the highest temperatures (Model 4), while near the Mercury's orbit in the model with the lowest temperatures (Model 3). Because temperatures along the surface, T_s, are smaller than T_m (Fig. 1b), the evaporation regions along the surface move to the inner side of the nebula ($r \approx 0.07$–0.15 AU; Fig. 3b). The temperature where iron dust evaporates completely ranges from 1315 K to 1384 K at the midplane and from 1376 K to 1569 K at the surface. The reason why metallic iron at the surface evaporates at a higher range of temperatures than at the midplane is that the density of metallic iron at the surface (eq. 6) at $f_{Fe} = 0$ is higher than that at the midplane (eq. 5). These temperatures are sufficiently smaller than the melting point of pure iron (1807 K; HANSEN and ANDERKO, 1958).

In the case of troilite, the ratios of sulfur in dust/(gas+dust), f_{FeS}, are plotted against r in Fig. 4 for the solar elemental ratios. Troilite dust particles survive to higher temperatures than that predicted by equilibrium calculations due to effects of evaporation kinetics. For example, in Model 3 along the midplane (Fig. 4a), sulfur starts to evaporate from troilite at $r \approx 0.95$ AU (0.01% evaporation) and evaporates completely with metallic iron residue at $r \approx 0.6$ AU in the case of equilibrium (the

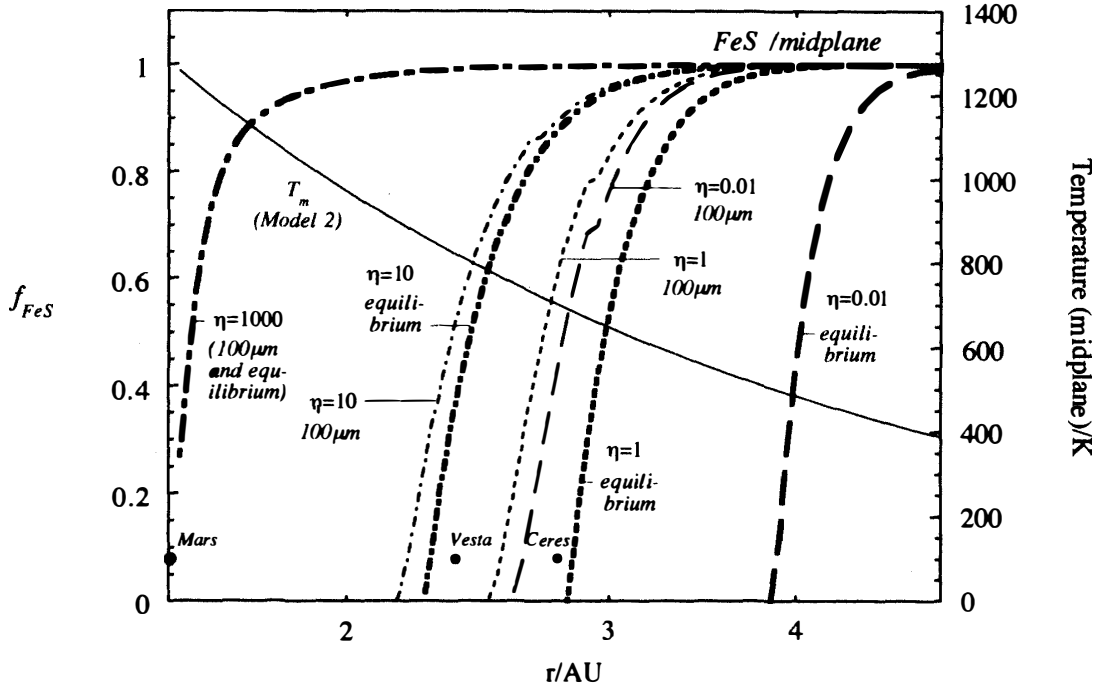

Fig. 6. The calculated dust/(dust+gas) ratios of FeS dust particles ($D_0 = 100\mu$m) at the midplane with different dust enrichment factor, η, based on Model 2. The equilibrium evaporation curves with different η's and temperatures of the midplane are also shown.

incongruent evaporation region is $r \approx 0.95$–0.6 AU), while the incongruent evaporation regions for 1 μm and 100 μm dust are $r \approx 0.9$–0.55 AU and 0.8–0.41 AU, respectively.

Comparison of the evaporation curves of metallic iron with those of troilite is shown in Fig. 5. In all the models, either along the midplane or surface, metallic iron evaporates always nearer to the sun than troilite even in Model 3, where the kinetic effect is largest. In other words, incongruent evaporation of troilite always occur to form metallic iron residue, and then both the residue and original dust of metallic iron evaporate in the inner region of the nebula as long as the dust falls along the midplane or the surface. Eutectic melting of troilite and metallic iron residue is not expected in all the models because the temperature where sulfur evaporates completely from troilite (704–991 K at the midplane, and 708–997 K at the surface) is sufficiently less than the eutectic point (1261 K; HANSEN and ANDERKO, 1958).

The evaporation kinetics of troilite under the dust enriched conditions ($\eta > 1$) is less effective than those with $\eta = 1$ (Fig. 6) although dust particles can survive to higher temperature regions. Troilite dust particles with $\eta = 1$, 10 and 614 can survive to 784, 904 and 1261 K (the eutectic temperature of Fe-FeS), respectively, in Model 2. In the case of $\eta = 1000$, troilite dust particles evaporates almost at equilibrium and about 30% of them can survive to 1261 K. The survived particles are probably melted at the point. On the contrary, the kinetic effect on evaporation of troilite dust particles with $\eta = 0.01$ are larger than those with $\eta = 1$, and they can survive to 756 K at 2.57 AU in the midplane, while the equilibrium evaporation temperature is 512 K at 3.8 AU in the midplane.

Metallic iron particles with $\eta = 0.01$, 1, 10 and 623 can survive to 1189, 1353, 1480 and 1808 K (the melting temperature of metallic iron), respectively. Even for dust particles with $\eta = 0.01$, the evaporation can be treated as equilibrium one.

6. Discussion

6.1. *Effects of evaporation kinetics of metallic iron*

There is little difference between the equilibrium evaporation curve and the evaporation curve with evaporation kinetics in all models. In other words, metallic iron dust evaporates so fast that the equilibrium is always maintained in the nebula, and few kinetic effects of evaporation are expected for the evaporation of metallic iron. The complete evaporation temperatures of metallic iron are consistent with the model temperatures assumed equilibrium conditions for the evaporation of opacity-bearing materials, and thus the present calculations confirm the validity of the assumption (1).

Metallic iron dust particles evaporate completely before melting except for highly dust-concentrated conditions ($\eta = 623$ in Model 2). YONEDA and GROSSMAN (1995) pointed out that the dust-enriched condition is necessary for a liquid phase to be stable although they aimed at the stability of CaO-MgO-Al_2O_3-SiO_2 melt. The present result is consistent with their results.

The presence of Ni or C in metal lowers the melting temperature. The minimum in the Fe-Ni liquidus curve is about 1700 K and the Fe-Fe_3C eutectic temperature is about 1420 K (HANSEN and ANDERKO, 1958). Small degree of melting might occur even in the case of $\eta = 1$ if C is present.

6.2. Effects of evaporation kinetics of troilite

Troilite dust particles evaporate completely in the region where $H_2S\,(g)$ is a dominant gas species for the evaporation. In other words, evaporation as $S_2\,(g)$ (and $HS\,(g)$) hardly occur.

A degree of the kinetic effect is largest in Model 3, smallest in Model 1, and moderate in Models 2 and 4 in accordance with v_r (Figs. 1c and 4). Evaporation rates are so slow that the equilibrium is not maintained as in the case of Model 3 (Fig. 1c). However, the kinetic effects are not so large except for Model 3. Thus, it can be regarded in general that incongruent evaporation of troilite occurs roughly under nearly equilibrium conditions in the nebula. TACHIBANA and TSUCHIYAMA (1998) proposed that kinetic constraints by a surface reaction are large for incongruent evaporation of sulfur from troilite as $H_2S\,(g)$. In fact, the evaporation coefficient, α_{H_2S}, estimated from their experiments are extremely small (about 10^{-3}). On the contrary, the kinetic effects on the evaporation of the moving dust in the nebula is expected to be small. This is because their drift velocities, v_r, are so small that the equilibrium is roughly maintained.

The evaporation kinetics of troilite under the dust enriched conditions ($\eta=1$) is less effective than those with $\eta=1$, while the kinetic effect is larger in the case of $\eta=0.01$. This is because a small degree of evaporation of each particles is enough to achieve the equilibrium under the dust enriched conditions, while each particle should evaporate a lot to achieve the equilibrium in the case of $\eta=0.01$.

6.3. General aspect of the effect of evaporation kinetics

When we consider the effect of the evaporation kinetics of dust particles moving in the nebula, it is convenient to compare the timescale imposed by the kinetics of evaporation with the timescales for radial and vertical drifts and that for coagulation.

When dust particles are coupled with nebular gas, the effect of ambient gas on the evaporation rate should be taken into account (Eqs. (8) and (12)). Discussion of kinetic timescale for evaporation, τ, was originally considered for evaporation of forsterite dust in the nebula by NAGAHARA and OZAWA (1996) and TSUCHIYAMA *et al.* (1999). The timescale, τ, is obtained from an evaporation rate, grain size, and the following dimensionless parameter, n'_e (TSUCHIYAMA *et al.*, 1999);

$$n'_e = 1 - \frac{p^e_E}{N_d kTn_0}, \tag{25}$$

where n_0 is the initial number of E atoms (or molecules) in a dust particle, and N_d is the number density of dust. τ is divided into two different ones. One is the timescale for complete evaporation, τ_{ev} ($n'_e<0$), and the other is that for equilibration after partial evaporation, τ_{eq} ($0<n'_e\leq 1$) (the timescale of 99.9% equilibration was adopted as τ_{eq} in the present study). In the case of $n'_e=0$, it takes an infinite time for complete evaporation. τ's for metallic iron and troilite along the midplane ($\eta=1$, $D_0=1\,\mu$m) are plotted against the distance from the sun, r, in Figs. 7a and 7b, respectively. The singularities in log τ curves correspond to $n'_e=0$, and the equilibrium evaporation

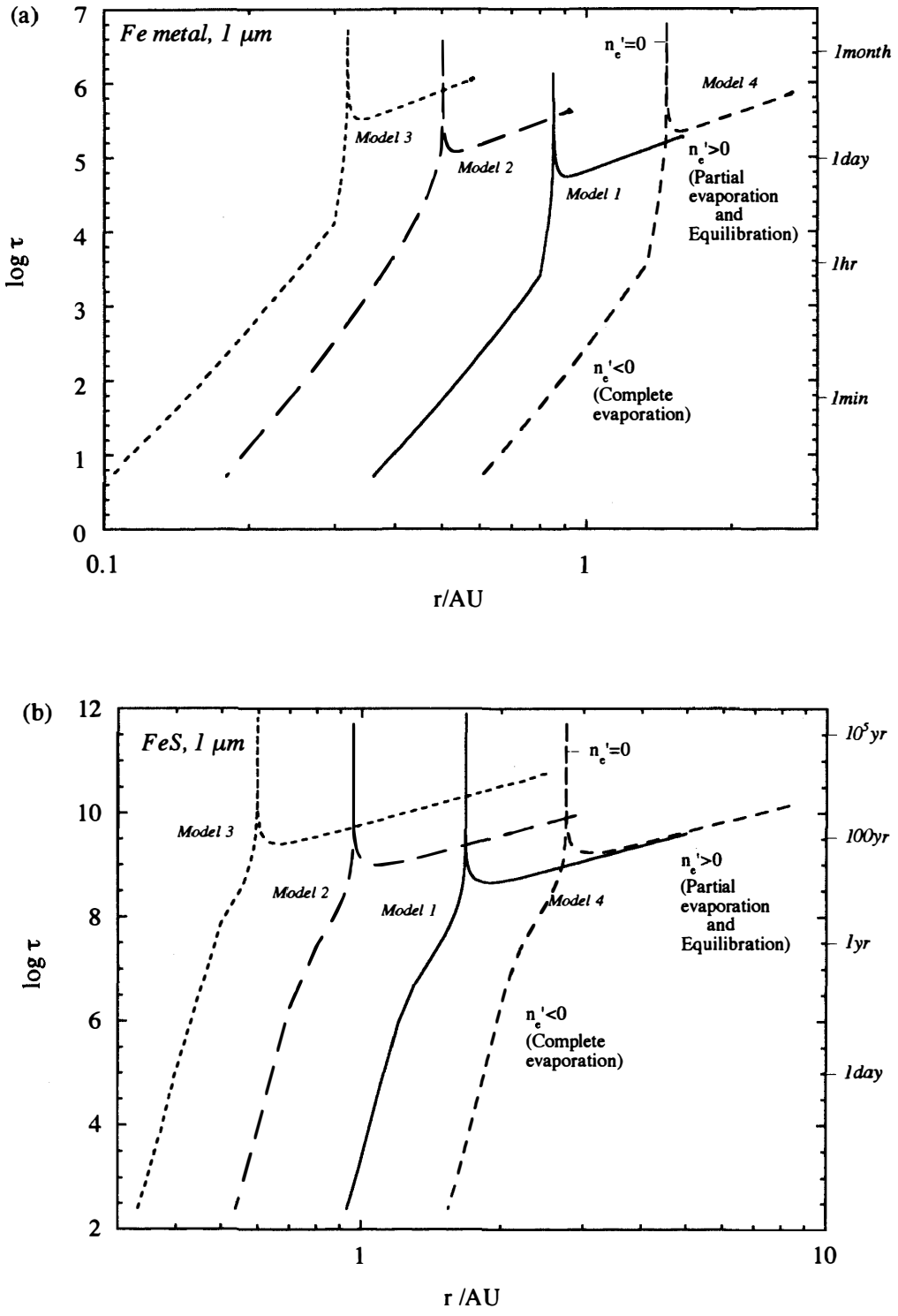

Fig. 7. The timescale for evaporation, τ, of 1 μm-sized dust particles with $\eta=1$ plotted against r. (a) Fe. (b) FeS. Singularity in each curve corresponds to the equilibrium complete evaporation point. The right side of the singularity corresponds to the region of equilibration after partial evaporation ($n'_e>0$), while the left side corresponds to the region of complete evaporation ($n'_e<0$).

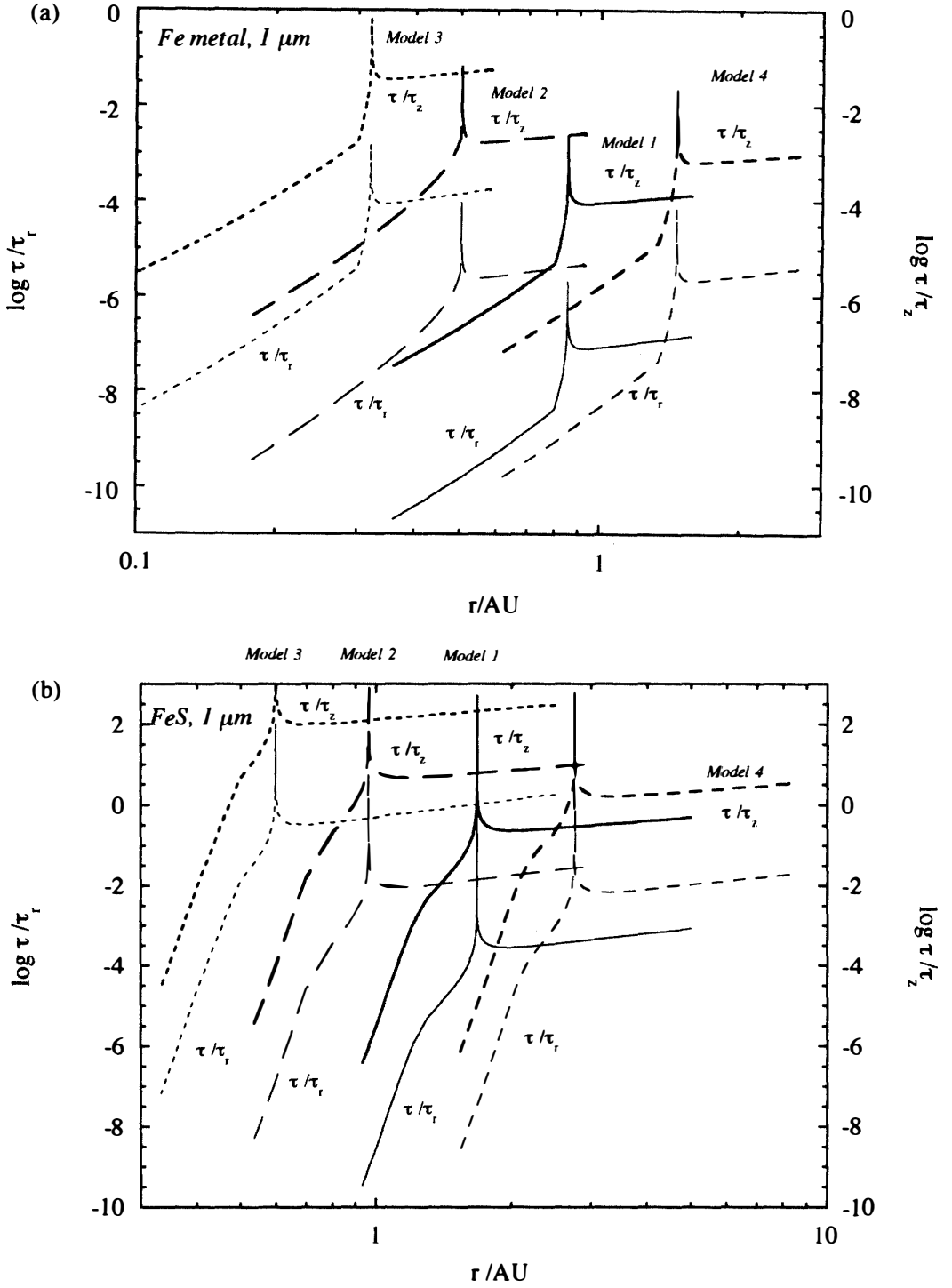

Fig. 8. The comparison of τ with the timescale for drifts along r- and z-directions, τ_r and τ_z, respectively. Thick lines express τ/τ_z curves (a) Fe ($D_0=1\,\mu m$). (b) FeS ($D_0=1\,\mu m$). (c) Fe ($D_0=100\,\mu m$).

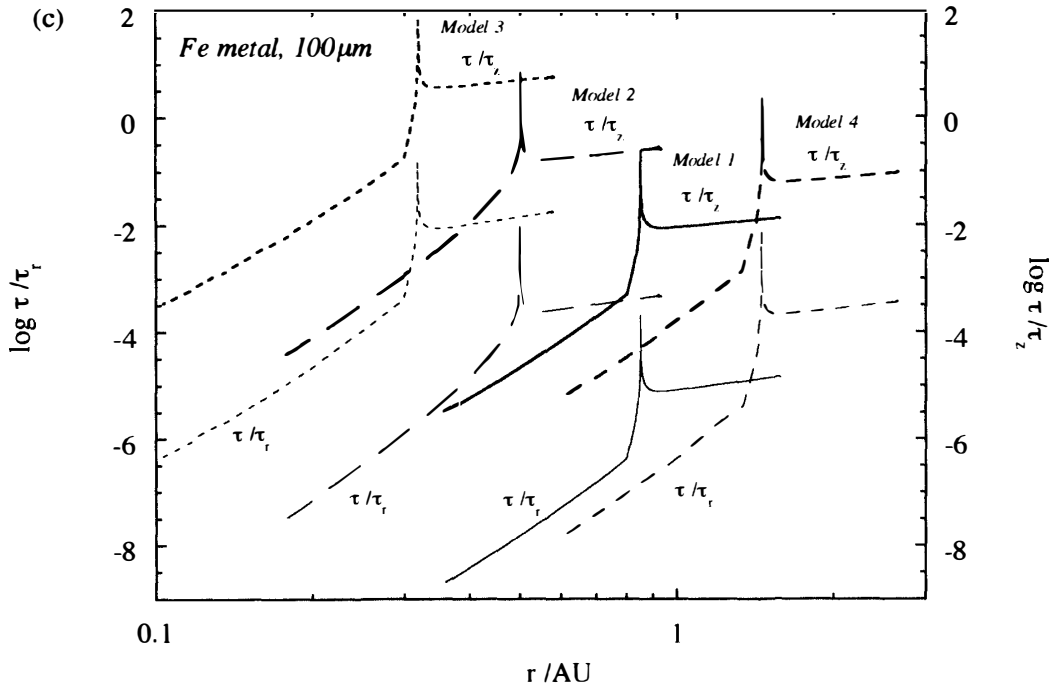

Fig. 8 (continued).

temperatures (f_{Fe}, $f_{FeS}=0$ in equilibrium calculation curves in Figs. 3–5). It is found that τ for metallic iron is shorter than τ for troilite because kinetic constraints for evaporation of metallic iron are smaller than those for evaporation of troilite.

The timescales for radial (r-direction) and vertical (z-direction) drifts of a dust particle coupled with gas are expressed by

$$\tau_r=\left|\frac{r}{v_r}\right|, \text{ and } \tau_z=\left|\frac{h}{v_z}\right|, \tag{26}$$

respectively, where v_z is the velocity of gas and dust moving along z-direction. We adopt the typical turbulent velocity as v_z ;

$$v_z\approx v_{\text{turbulence}}\approx\alpha_v^{3/5}c_s=\alpha_v^{3/5}\sqrt{\gamma\frac{k}{\mu}\frac{T_m+T_S}{2}}, \tag{27}$$

where c_s is the approximated sound velocity in the nebula.

The evaporation timescales, τ, for metallic iron and troilite with $D_0=1\,\mu$m are compared with τ_r and τ_z in Figs. 8a and 8b, respectively. The case for metallic iron with $D_0=100\,\mu$m is also shown in Fig. 8c. Figure 8a shows that τ for metallic iron is always shorter than τ_z, and much shorter than τ_r. This indicates that the evaporation kinetics does not work effectively for metallic iron dust particles even along the z-direction. This is consistent with the present calculation at least for the radial movement (Fig. 3a).

In the case of troilite, τ is shorter than τ_r in Models 1, 2 and 4, and comparable to

τ_r in Model 3 ($0<n'_e\leq 1$) (Fig. 8b). This means that the evaporation kinetics works along r-direction only in Model 3. This is also consistent with the present result (Fig. 4a). On the other hand, τ is comparable to τ_z in Models 1, 2 and 4, and larger than τ_z in Model 3. This implies that the effect of the evaporation kinetics can be expected for troilite dust particles moving along z-direction.

We can discuss the dependence of τ/τ_r and τ/τ_z on grain size as well. τ changes almost linearly with the grain size (TSUCHIYAMA *et al.*, 1999), while τ_r *and* τ_z would be constant irrespective of grain size as long as dust particles are small enough to couple with gas ($\leq 100\mu$m). Thus, τ/τ_r and τ/τ_z have a linear dependence on the grain size (Figs. 8a and c). Judging from Fig. 8c, the kinetic effect along r-direction cannot be expected for metallic iron with $D_0=100\mu$m ($\log \tau/\tau_r \ll 0$), and this is consistent with the present calculation (Fig. 3a), while the kinetics might work more or less for the z-direction movement in Model 2, 3 and 4. The similar discussion can be made for troilite with $D_0=100\mu$m, and the kinetic effect of evaporation can be expected both along r- and z-directions as shown in Fig. 4a for r-direction.

The timescale for coagulation, τ_c, is estimated from the time during which the size of a particle is doubled by collisional growth (WATANABE and IDA, 1997) ;

$$\tau_c=\frac{4}{\beta}\left(\frac{\tilde{\rho}}{\rho_d}\right)\left(\frac{D}{\Delta v}\right), \tag{28}$$

where β is a sticking probability, $\tilde{\rho}$ is a material density of a dust particle, and Δv is a collisional velocity. For dust particles with $D_0=1\mu$m at 1 AU, τ_c ranges from 10^{-4} to

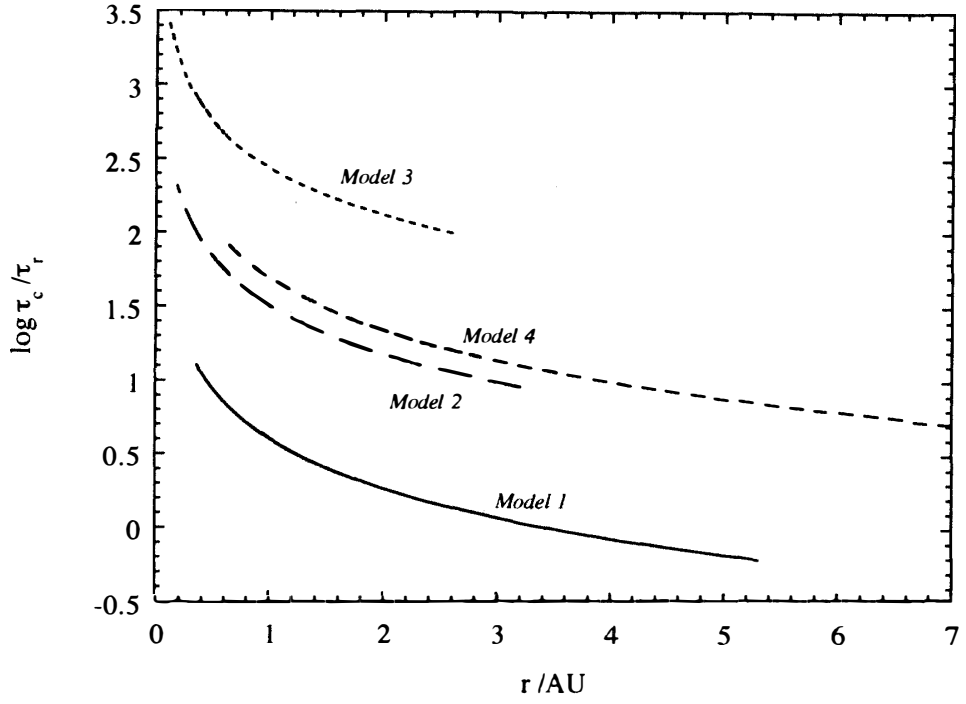

Fig. 9. The comparison of the timescale of coagulation (10^5yr), τ_c, with the timescale for radial drift, τ_r.

10^{-6} τ_r in Models 1–4 if perfect sticking ($\beta=1$) is assumed although the collisional behavior of dust aggregates has been poorly known. The τ_c values for 1 μm-sized dust indicate that dust particles should grow at the same distance from the sun until τ_c becomes comparable to τ_r. A 1 μm-sized dust grain would grow rapidly up to several tens cm at 1 AU. If such large dust aggregates (~several tens cm) were formed, they could be decoupled with gas and drift to the sun faster than gas. If this is the case, τ and τ_r would become longer and shorter, respectively, and they would make τ/τ_r large enough to expect large kinetic effects on evaporation.

However, in the strong turbulent nebula, collision is likely to break a particle, and prevent it from growing. Thus, β in the turbulent nebula might be much smaller than unity (perfect sticking). We consider the case where β was so small that dust particles could not grow by mutual collision until the turbulence weakened. We adopt the lifetime of the turbulent disk (10^5–10^6 yr) as τ_c here. Log (τ_c/τ_r) in Models 1–4 are plotted in Fig. 9. It is found that τ_c is longer than τ_r. Thus, coagulation can be negligible, and the large kinetic effects due to coagulation cannot be expected as long as turbulence prevent dust particles from growing. Again, note that little is known about the collisional behavior of dust aggregates, and it should be investigated in more detail.

6.4. *Fe/S fractionation*

Fe/S fractionation can be discussed from the evaporation curves as schematically shown in Fig. 10. The Fe/S ratios of solid components (dust) change within the incongruent evaporation range of troilite (Region (A) in Fig. 10). If the sold-gas separation occurred effectively, Fe/S fractionation could be expected in Region (A). If the solid component in this region accreted into chondritic parent bodies, they would have had higher Fe/S ratios than that of the solar abundance.

The Fe/S ratios of gas components change within the congruent evaporation range of metallic iron (Region (B) in Fig. 10). If all solid components accreted faster to the sun than gas components, the gas components with various Fe/S ratios would be left behind in this region. Dust particles might grow by collision and had larger drift velocity than gas, although we ignored the growth of dust in the present calculations. If the residual gas components (Fe(g) and S-bearing gas) recondensed into solids by cooling, the recondensed solid phase should have various Fe/S ratios in this region. If parent bodies of meteorites and planets were formed from such recondensed solids, some of them would have lower Fe/S values than that of the solar abundance. However, this cannot explain the compositions of chondrites and probably terrestrial planets, which have higher Fe/S values than the solar abundance (*e.g.*, DODD, 1981; WASSON and KALLEMEYN, 1988).

LEWIS (1972) discussed the elemental fractionation in the primordial solar nebula based on the equilibrium condensation model. He concluded that the density variation of the terrestrial planets could be explained by the difference of the accretion temperature as a function of the distance from the protosun. He pointed out that the accretion temperature of Mercury was so high that metallic iron and only refractory silicates condensed, while that of Mars was low enough for condensation of troilite, Fe-bearing silicates, and hydrous silicates. He proposed that Fe/S fractionation had occurred in the region between Earth and Mars. However, he did not take account of the dynamic

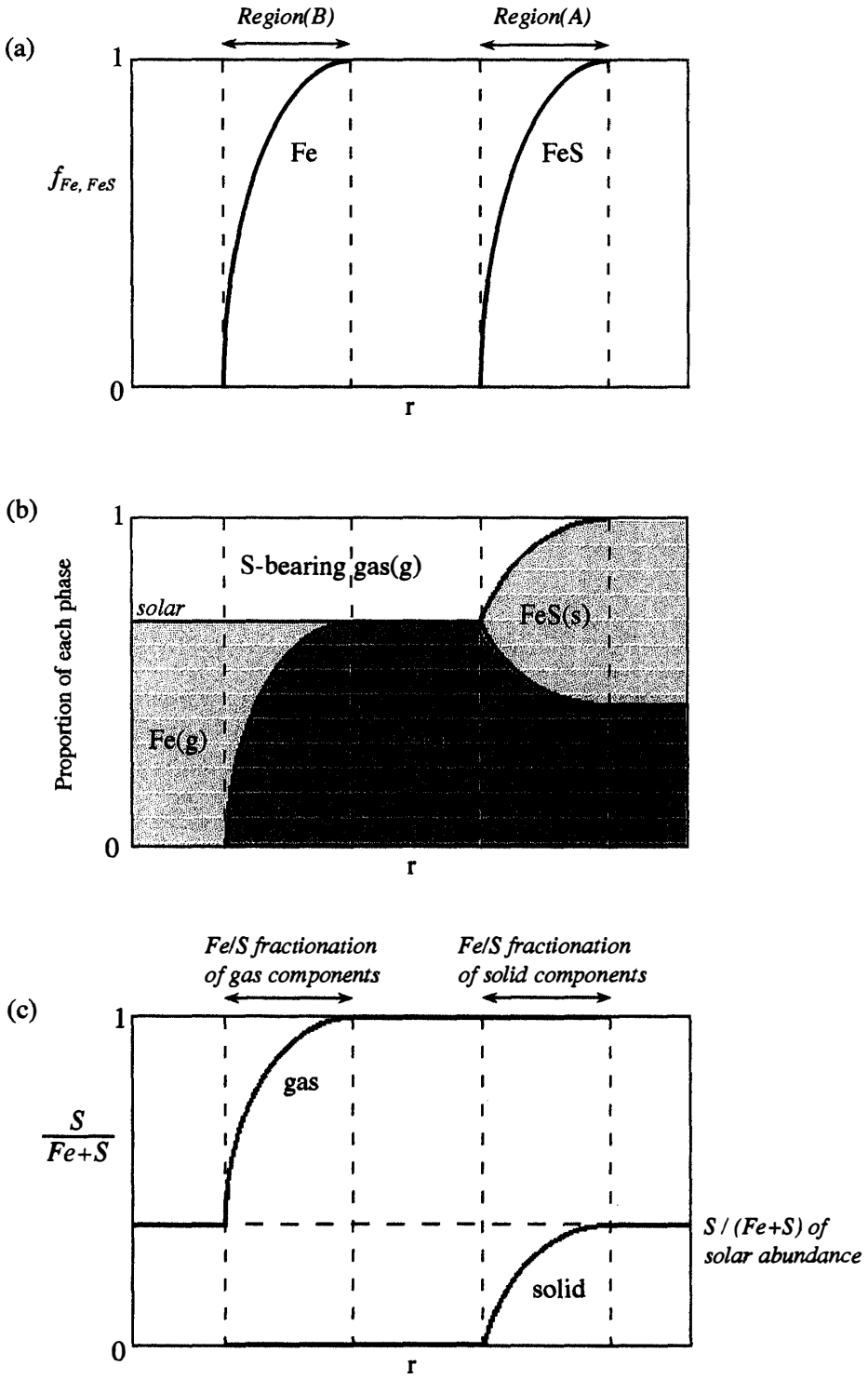

Fig. 10. A schematic drawing for explaining Fe/S fractionation in the primordial solar nebula. (a) f_{Fe}-r and f_{FeS}-r curves. Troilite evaporates incongruently in Region (A), and metallic iron evaporates in Region (B). (b) The change in the proportion of each phase by the evaporation of metallic iron and troilite plotted against r. (c) The change in the ratio of S/(Fe+S) of solid and gas components plotted against r. In Region (A), S/(Fe+S) of solid components changes by incongruent evaporation of troilite, and thus Fe/S fractionation of solid components is expected. In Region (B), S/(Fe+S) of gas components changes by evaporation of metallic iron.

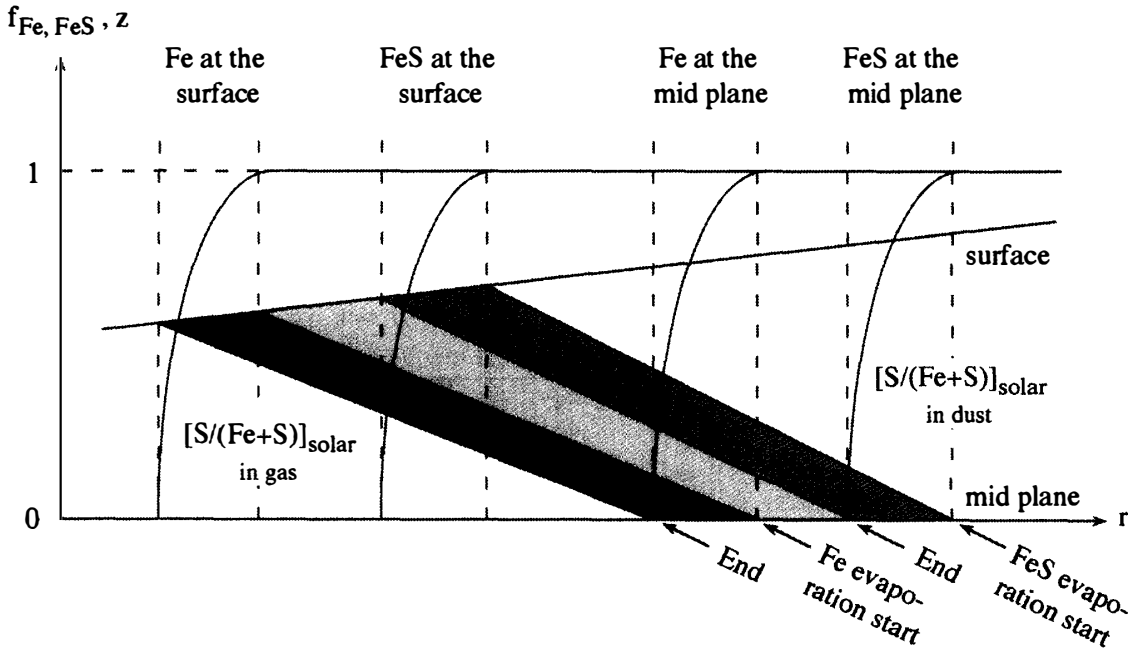

Fig. 11. A schematic illustration of the r- and z-direction structure of the solar nebula with f_{Fe}-r and f_{FeS}-r curves. If the z-direction movement is also taken into account, mixing of material at the surface and the midplane would make wide variations in the gas and solid component, respectively, throughout the nebula.

movement of dust in the nebula, elemental fractionation in the z-direction, or the time evolution of the nebula. The equilibrium approximation appears to be useful for the elemental fractionation only along r-direction as our results suggest. However, dust particles and gas, in fact, move along z-direction by turbulence. Since the temperatures of the surface are much lower than those of the midplane, dust particles can survive in the inner region of the nebula near the surface even if the temperature of the midplane is higher than their evaporation temperature. Movement of dust particles along z-direction could cause Fe/S fractionation in a wider range of the nebula than the range proposed by LEWIS (1972).

Although the movement of dust along z-direction was not calculated numerically in the present models, a rough estimation for Fe/S fractionation in the entire nebula could be made (Fig. 11). As in Fig. 8a, the effect of the evaporation kinetics on metallic iron is probably small for z-direction movement as well. Thus, evaporation of metallic iron may be deemed as the equilibrium one along z-direction as well. In the case of troilite, the effect of evaporation might work somehow for z-direction movement (Fig. 8b). If $\tau \gg \tau_z$, the nebula would be well-mixed by turbulence, and the fractionation in z-direction would be diminished. However, Fig. 8b shows that τ is comparable to τ_z for 1 μm-sized troilite dust. This implies that the kinetic effect may not make the nebula well-mixed in z-direction but make the position of the evaporation lines drawn in Fig. 11 ambiguous. Hence, Fig. 11 is approximately valid for a rough estimation of Fe/S fractionation in the nebula.

Fe/S fractionation should occur within the range between the regions where troilite

particles begin to evaporate at the midplane and evaporate completely at the surface if the separation of solid component is taken into consideration. These fractionation ranges are about 0.1–3 AU, and especially in Model 4, the range is so wide that the asteroid belt and four terrestrial planets are included (Fig. 5d). This range is much wider than that proposed by LEWIS (1972). Mixing of materials at the surface and the midplane by the turbulence would make wide variations in the gas and solid component, respectively, in the wide range of the nebula.

The possibility of elemental fractionation during condensation and/or coagulation process in the cooling nebula should be also considered. In the active stage (10^5–10^6 yr), the strong turbulence would prevent the growth of dust particles as mentioned above. Then, the disk turns to the passive disk stage by the stop of the accretion into the disk from the molecular cloud. It is considered that planets and parent bodies of meteorites were formed at the passive disk stage. There is still controversy on the formation mechanism of planetesimals. Some researchers are in favor of the gravitational instability (*e.g.*, HAYASHI *et al.*, 1985; WATANABE and IDA, 1997), while others are for the simple collisional growth. (*e.g.*, WEIDENSCHILLING, 1980; WEIDENSCHILLING and CUZZI, 1993).

As for refractory elements, the elemental fractionation caused by evaporation and condensation in the passive disk might be ineffective because the passive disk was not presumably so energetic, and thus the elemental patterns of refractory elements in chondrites might reflect the elemental fractionation at the last stage of the active nebula. As for moderately volatile elements, it might be of importance to consider the elemental fractionation in the passive disk because their evaporation and/or condensation take place at lower temperatures. Sulfur is moderately volatile, and might have been fractionated to make a monotonically depleted abundance pattern of moderately volatile elements during coagulation as suggested by CASSEN (1996). CASSEN (1996) discussed the fractionation of moderately volatile elements during coagulation with taking the escape of nebular gas into consideration, and proposed that the monotonic abundance patterns of moderately volatile elements in CO and CV chondrites was successfully reproduced. However, the depletion pattern of moderately volatiles might be explained by our model as well. If the evaporation and condensation of moderately volatile elements occurred nearly in equilibrium as well as sulfur, z-direction mixing of the nebula might be able to establish their depletion pattern monotonically with volatility. The kinetic data are too scarce to discuss this in detail.

The present calculations for the active disk can be regarded as the starting point for the simulation of elemental fractionation in the nebula, or a chemical evolution of the primordial solar nebula. Problems to be resolved are follows; (1) movement of dust particles along z-direction due to turbulence and accompanied evaporation and condensation of dust should be examined, (2) growth of dust particles due to collision which causes the differences between drift velocities of dust and gas should be examined to elucidate the separation of evaporated gas and dust, and finally (3) the evolution of the turbulent primordial solar nebula should be considered to discuss the observed (or estimated) Fe/S ratios of meteorites and terrestrial planets.

7. Conclusion

(1) The evaporation kinetics of metallic iron and troilite, which were experimentally determined (TSUCHIYAMA and FUJIMOTO, 1995; TACHIBANA and TSUCHIYAMA, 1998), was combined to the recent protoplanetary disk model (WATANABE and IDA, 1997) to understand the evaporation of metallic iron and troilite moving radially to the sun in the turbulent solar nebula. It was found that metallic iron would evaporate almost in equilibrium. In the case of troilite, the dust would survive to higher temperatures than the equilibrium evaporation temperature due to its slow evaporation rate. However, the kinetic effects are not so large that evaporation would take place roughly in equilibrium.

(2) The evaporation behaviors of metallic iron and troilite under dust enriched conditions were also examined. The kinetic effects are also negligible under dust enrichment conditions. However, dust enrichment would increase the equilibrium evaporation temperature and cause the melting of dust particles (melting of metallic iron and Fe-FeS eutectic melting) when the density of dust was ~ 1000 times larger than that for the solar elemental abundance.

(3) The timescale for evaporation, τ, was compared with the timescales for radial (r-direction) and vertical (z-direction) drifts, τ_r and τ_z, and the timescale for coagulation, τ_c, to understand general aspects of evaporation in the solar nebula. τ for metallic iron with initial radius of less than 100μm is generally shorter than τ_r and τ_z. This implies that the kinetic effect cannot be expected for metallic iron moving in the turbulent nebula. τ for troilite is shorter than or comparable to τ_r, while comparable to or larger than τ_z. The evaporation kinetics would work more or less along r-direction, and the effect of evaporation kinetics can be expected along z-direction. The above rough estimation is consistent with the present numerical calculations along r-direction. The timescale for coagulation, τ_c, is longer than τ_r and τ_z provided that the strong turbulence in the nebula prevented dust particles from growing. If this is the case, coagulation can be negligible in the present discussion.

(4) The rough estimation for Fe/S fractionation throughout the nebula was made based on the present results. Along r-direction, the distribution of Fe/S ratios in gas and solid phase would be almost the same as the equilibrium distribution. Along z-direction, it would be different from the equilibrium one because of $\tau \geq \tau_z$ for troilite. However, τ_z is not short enough to mix the nebula along z-direction and make it unfractionated. Hence, the Fe/S ratio along z-direction would be determined by the temperature distribution along z-direction and the gas-solid reaction kinetics. By taking the temperature distribution along z-direction into consideration, the range within which the Fe/S fractionation is expected would become larger than the range proposed by previous studies.

Acknowledgments

This research is supported by a Grant-in Aid for Scientific Research from the Ministry of Education of Japan No. 07454132 and Hyogo Science and Technology

Association. The authors are grateful to Dr. P. CASSEN and an anonymous reviewer for their helpful reviews.

References

ANDERS, E. and GREVESSE, N. (1989): Abundance of the elements: Meteoritic and solar. Geochim. Cosmochim. Acta, **53**, 197–214.

CAMERON, A.G.W. (1973): Accumulation processes in the primitive solar nebula. Icarus, **18**, 407–450.

CAMERON, A.G.W. and FEGLEY, M.B. (1982): Nucleation and condensation in the primitive solar nebula. Icarus, **52**, 1–13.

CARMICHAEL, R.S. (1989): Physical Properties of Rocks and Minerals. CRC Press, 741 p.

CASSEN, P. (1996): Models for the fractionation of moderately volatile elements in the solar nebula. Meteorit. Planet. Sci., **31**, 793–806.

CHASE, M.W.J., DAVIES, C.A., DOWNEY. J.R., Jr., FRURIP, D.J., MCDONALD, R.A. and SYVERUND, A.N. (1985): JANAF Thermochemical Tables, 3rd ed. National Bureau of Standards, U.S.A., 1856 p.

CUZZI, J.N., DOBROVOLSKIS, A.R. and HOGAN, R.C. (1996): Turbulence, chondrules, and planetesimals. Chondrules and Protoplanetary Disk, ed. by R.H. HEWINS *et al.* Cambridge, Cambridge Univ. Press, 35–43.

DODD, R.T. (1981): Meteorites. Cambridge, Cambridge Univ. Press, 368 p.

GROSSMAN, J.N. and WASSON, J.T. (1982): Evidence for primitive nebular components in chondrules from the Chainpur chondrite. Geochim. Cosmochim. Acta, **46**, 1081–1099.

GROSSMAN, J.N. and WASSON, J.T. (1983): Refractory precursur components of Semarkona chondrules and the fractionation of refractory elements among chondrites. Geochim. Cosmochim. Acta, **47**, 759–771.

GROSSMAN, L. (1972): Condensation in the primitive solar nebula. Geochim. Cosmochim. Acta, **36**, 597–619.

GROSSMAN, L. and LARIMER, J. (1974): Early chemical history of the solar system. Rev. Geophys. Space Phys., **12**, 71–101.

HAACK, H. and SCOTT, E.R.D. (1993): Nebula formation of the H, L, and LL parent bodies from a single batch of chondritic materials (abstract). Meteoritics, **28**, 358–359.

HANSEN, M. and ANDERKO, K. (1958): Constitution of Binary Alloys. NewYork, McGraw-Hill, 1305 p.

HAYASHI, C., NAKAZAWA, K. and Nakagawa, Y. (1985): Formation of the solar system. Protostars & Planets II, ed. by D.C. BLACK and M.S. MATTHEWS. Tucson, Univ. Arizona Press, 1100–1153.

HIRTH, J.P. and POUND, G.M. (1963): Condensation and Evaporation, Nucleation and Growth Kinetics. Pergamon Press, 191 p.

IMAE, N. and KITAMURA, M. (1995): Sulfidation of metallic iron in the primordial solar nebula. Proc. NIPR Symp. Antarct. Meteorites, **8**, 139–151.

KERRIDGE, J.F. and MATTHEWS, M.S. (1988): Meteorites and the Early Solar System. Tucson, Univ. Arizona Press, 1269 p.

LARIMER, J.W. and ANDERS, E (1967): Chemical fractionation in meteorites - II. Abundance patterns and their interpretation. Geochim. Cosmochim. Acta, **31**, 1239–1270.

LARIMER, J.W. and ANDERS, E (1970): Chemical fractionation in meteorites-III. Major element fractionations in chondrites. Geochim. Cosmochim. Acta, **34**, 367–387.

LAURETTA, D.S. (1997): Theoretical and experimental studies of iron-nickel-sulfur, beryllium, and boron cosmochemistry. Ph. D Thesis, Washington University.

LAURETTA, D.S., KREMSER, D.T and FEGLEY, B., Jr. (1996): The rate of iron sulfide formation in the solar nebula. Icarus, **34**, 288–315.

LAURETTA, D.S., LODDERS, K. and FEGLEY, B., Jr. (1997): Experimental simulations of sulfide formation in the solar nebula. Science, **277**, 358–360.

LEWIS, J.S. (1972): Metal/silicate fractionation in the solar system. Earth Planet. Sci. Lett., **15**, 286–290.

LEWIS, J.S. (1995): Physics and Chemistry of the Solar System. Academic Press, 556 p.

LYNDEN-BELL, D. and PRINGLE. J.E. (1974): The evolution of viscous discs and the origin of the nebular variables. Mon. Not. R. Aston. Soc., **168**, 603–637.

MORFILL, G.E., TSCHANUTER, W. and VÖLK, H.J. (1985): Dynamical and chemical evolution of the protoplanetary nebula. Protostars & Planets II, ed. by D.C. BLACK and M.S. MATTHEWS. Tucson, Univ. Arizona Press, 493–533.

NAGAHARA, H. and OZAWA, K (1996): Evaporation of forsterite in H_2 gas. Geochim. Cosmochim. Acta, **60**, 1445–1459.

PALME, H., LARIMER, J.S. and LIPSCHUTZ, M.E. (1988): Moderately volatile elements. Meteorites and the Early Solar System, ed. by J.F. KERRIDGE and M.S. MATTHEWS. Tucson, Univ. Arizona Press, 436–458.

PAULE, R.C. and MARGRAVE, J.L. (1967): Free-evaporation and effusion techniques. The Characterization of High-Temperature Vapors, ed. by J.L. MARGRAVE. J. Wiely, 436–461.

RUDEN, S.P. and POLLACK, J.B. (1991): The dynamical evolution of the protosolar nebula. Astrophys. J., **375**, 740–760.

SEARS, D.W.G., HUANG, S. and BENOIT, P.H. (1996): Open-system behaviour during chondrule formation. Chondrules and Protoplanetary Disk, ed. by R.H. HEWINS *et al.* Cambridge, Cambridge Univ. Press, 221–231.

SCOTT, E.R.D. and HAACK, H. (1993): Chemical fractionation in chondrites by aerodynamic sorting of chondritic materials (abstract). Meteoritics, **28**, 434.

SHU, F.H., ADAMS, F.C. and LIZANO, S. (1987): Star formation in molecular clouds: Observation and theory. Ann. Rev. Astron. Astrophys., **25**, 23–81.

TACHIBANA, S. and TSUCHIYAMA, A. (1998): Incongruent evaporation of troilite (FeS) in the primordial solar nebula; An experimental study. Geochim. Cosmochim. Acta, **62**, 2005–2022.

TSUCHIYAMA, A. and FUJIMOTO, S. (1995): Evaporation experiments of iron in vacuum. Proc. NIPR Symp. Antarct. Meteorites, **8**, 205–213.

TSUCHIYAMA, A., UYEDA, C. and MAKOSHI, Y. (1997) Incongruent evaporation experiments on iron sulfide ($Fe_{1-\delta}S$) under H_2-rich (at 1 atm) and evacuated conditions. Geochem. J., **31**, 289–302.

TSUCHIYAMA, A., TACHIBANA, S. and TAKAHASHI, T. (1999): Evaporation of forsterite in the primordial solar nebula; rates and accompanied isotopic fractionation. submitted to Geochim. Cosmochim. Acta.

WASSON, J.T. and KALLEMEYN, G.W. (1988): Compositions of chondrites. Philos. Trans. R. Soc. London, **A325**, 535–544.

WATANABE, S. and IDA, S. (1997): Hikaku wakuseikei keiseiron (Comparative theory on the formation of planetary systems). Hikaku Wakuseigaku (Comparative Planetology), ed. by T. MATSUI *et al.* Tokyo, Iwanami, 131–231 (in Japanese).

WEIDENSCHILLING, S.J. (1980): Dust to planetesimals: settling and coagulation in the solar nebula. Icarus, **44**, 172–189.

WEIDENSCHILLING, S.J. and CUZZI, J.N. (1993): Formation of planetesimals in the solar nebula. Protostars & Planets III, ed. by E.H. LEVY and J.I. LUNINE. Tucson, Univ. Arizona Press, 1031–1060.

WOOD, J.A. and HASHIMOTO, A. (1993): Mineral equilibrium in fractionated nebular systems. Geochim. Cosmochim. Acta, **57**, 2377–2388.

YAMAMOTO, T. and HASEGAWA, H. (1977): Grain formation through nucleation process in astrophysical environment. Prog. Theor. Phys., **58**, 816–828.

YONEDA, S. and GROSSMAN, L. (1995): Condensation of CaO-MgO-Al_2O_3-SiO_2 liquid from cosmic gases. Geochim. Cosmochim. Acta, **59**, 3413–3444.

(Received November 2, 1998; Revised manuscript accepted February 4, 1999)